Bulletin of Mathematical Biology (2021) 83:42
https://doi.org/10.1007/s11538-021-00869-5

Society for Mathematical Biology

ORIGINAL ARTICLE

Modeling CAR T-Cell Therapy with Patient Preconditioning

Katherine Owens[1] · **Ivana Bozic**[1]

Received: 19 June 2020 / Accepted: 11 February 2021 / Published online: 19 March 2021

Abstract

The Federal Drug Administration approved the first Chimeric Antigen Receptor T-cell (CAR T-cell) therapies for the treatment of several blood cancers in 2017, and efforts are underway to broaden CAR T technology to address other cancer types. Standard treatment protocols incorporate a preconditioning regimen of lymphodepleting chemotherapy prior to CAR T-cell infusion. However, the connection between preconditioning regimens and patient outcomes is still not fully understood. Optimizing patient preconditioning plans and reducing the CAR T-cell dose necessary for achieving remission could make therapy safer. In this paper, we test treatment regimens consisting of sequential administration of chemotherapy and CAR T-cell therapy on a system of differential equations that models the tumor-immune interaction. We use numerical simulations of treatment plans from within the scope of current medical practice to assess the effect of preconditioning plans on the success of CAR T-cell therapy. Model results affirm clinical observations that preconditioning can be crucial for most patients, not just to reduce side effects, but to even achieve remission at all. We demonstrate that preconditioning plans using the same CAR T-cell dose and the same total concentration of chemotherapy can lead to different patient outcomes due to different delivery schedules. Results from sensitivity analysis of the model parameters suggest that making small improvements in the effectiveness of CAR T-cells in attacking cancer cells will significantly reduce the minimum dose required for successful treatment. Our modeling framework represents a starting point for evaluating the efficacy of patient preconditioning in the context of CAR T-cell therapy.

Keywords ODE model · Tumor-immune interaction · Chimeric antigen receptor T-cells · Combination treatment · Preconditioning

✉ Ivana Bozic
ibozic@uw.edu

[1] Department of Applied Mathematics, University of Washington, Seattle, WA, USA

1 Introduction

1.1 CAR T-Cell Therapy

Cancer treatment plans often draw upon multiple treatment modalities, including surgery, radiation, chemotherapy, and immunotherapy, in order to combat disease (Miller et al. 2019; Mokhtari et al. 2017; Palmer and Sorger 2017; Khalil et al. 2016; Yamamoto et al. 2016). Immunotherapies aim to enhance the body's natural defense mechanisms against tumor cells. Immunotherapy approaches include injections of molecules that promote immune activity like interleukins, antibodies, checkpoint inhibitors, and vaccines, as well as adoptive cellular therapies (ACT) in which T-cells are isolated from the patient, expanded ex vivo, and then reintroduced into the patient (Kruger et al. 2019).

Advances in gene-editing during the 1990s enabled a new type of ACT in which a patient's T-cells are genetically engineered to recognize markers displayed on the surface of tumor cells (Almåsbak et al. 2016). These genetically engineered T-cells, called CAR T-cells, were first reported to effectively eradicate lymphoma cells in a murine model in 2010 (Kochenderfer et al. 2010). Following this breakthrough, CAR T-cell therapy showed dramatic success against lymphomas and leukemias in a series of clinical trials with complete remission rates in the range of 65–90% (Almåsbak et al. 2016). In late 2017, the FDA approved two CAR T-cell therapies for treatment of relapsed and refractory Acute Lymphoblastic Leukemia and for diffuse large B-cell lymphoma (June and Sadelain 2018). Continued advances in T-cell engineering, genetic editing, selection of targets, and cell manufacturing have the potential to broaden applications of CAR T-cell therapy to treat diseases beyond leukemia and lymphoma (Almåsbak et al. 2016; Brown and Mackall 2019; Pettitt et al. 2018).

Although CAR T-cell therapies show great promise in the fight against cancer, there are multiple challenges hindering their universal adoption, including potentially fatal inflammatory side effects that occur in up to 10% of patients who have positive responses to the infusion (Pettitt et al. 2018). The toxic side effects of CAR T-cell therapy include neurologic effects, B-cell aplasia, and cytokine release syndrome (CRS), ranging in severity from mild flu-like symptoms to death. Studies associate higher levels of tumor burden at the time of treatment with more serious side effects (Brown and Mackall 2019).

Under current medical practice, care providers administer a lymphodepleting round of chemotherapy prior to CAR T-cell injections in order to increase efficacy and reduce side effects of treatment (Mahadeo et al. 2019). It has been hypothesized that by reducing tumor burden and the number of normal immune cells, chemotherapy allows CAR T-cells to proliferate and overcome the cancer cells more easily. Though the use of such preconditioning regimens is common, the optimal combination of chemotherapy and CAR T-cells has not yet been determined. A mathematical model illustrating how these two forms of treatment interact for any given patient could help address this question.

1.2 Mathematical Modeling of Cancer Treatment

Systems of ordinary differential equations (ODEs) have been widely used to model tumor-immune interactions on the cell population level (Borges et al. 2014; de Pillis et al. 2005, 2006; Kirschner and Panetta 1998; Kuznetsov et al. 1994; Nanda et al. 2013; Pinho et al. 2002; Ribba et al. 2012; Rösch et al. 2016; Usher 1994). Many of these models also incorporate treatment via chemotherapy, immunotherapy or both. Several thorough reviews of non-spatial mathematical models of interactions between the immune system, tumor cells, and cancer therapies exist in the literature (Eftimie et al. 2011; Talkington et al. 2018).

Methods used to mathematically model cancer and the immune response range in complexity from using two differential equations to describe predator-prey-type dynamics between immune and tumor cells (Usher 1994; Kirschner and Panetta 1998; Kuznetsov et al. 1994; Sahoo et al. 2020; Talkington et al. 2018), up through detailed mechanistic models that explicitly represent multiple components of the immune response (Hardiansyah and Ng 2019; Harris et al. 2018; Ribba et al. 2012). Cancer therapy has been incorporated through simple time-independent dosing (Usher 1994; Kirschner and Panetta 1998; Pinho et al. 2002), as well as through more realistic time-dependent dose schedules (Pinho et al. 2002; de Pillis et al. 2006). Here, we aim to formulate a goldilocks model, incorporating just enough complexity to achieve expected biological outcomes and enable testing a range of medically relevant treatment plans (Brady and Enderling 2019).

Several computational models have recently been developed to investigate aspects of CAR T-cell therapy including cytokine release syndrome toxicity management (Hopkins et al. 2018; Stein et al. 2017, 2019), mechanisms of CAR T-cell activation (Harris et al. 2018; Rohrs et al. 2019), and how factors including CAR T-cell dose, donor-dependent T-cell differences, cancer cell proliferation, and target antigen expression contribute to the overall effectiveness of CAR T-cell therapy (Hardiansyah and Ng 2019; Kimmel et al. 2019; Rodrigues et al. 2019; Sahoo et al. 2020). Here, we formulate a model that allows us to investigate how the interplay between specific preconditioning plans and CAR T-cell dosage affects patient outcomes.

The remainder of the paper follows this general outline: In Sect. 2, we formulate a model for tumor-immune system interaction and detail how sequential combination of chemotherapy and CAR T-cell therapy is incorporated into the model. In Sect. 3, we evaluate numerical simulations of treatment plans that adhere to the FDA package inserts for the two approved CAR T-cell therapies (Kite 2017; Novartis 2017). As discussed in Sect. 4, these simulations show that appropriate chemotherapeutic preconditioning can reduce the CAR T-cell dosage necessary for a patient to achieve remission. Our results suggest that small changes in the delivery schedule of chemotherapy and CAR T-cell therapy can have a significant effect on the outcome of treatment.

2 Model Formulation

Here we formulate a model of the tumor-immune interaction by updating Kuznetsov's influential 1994 model (Kuznetsov et al. 1994). Our goal is to incorporate CAR T-cell treatment, chemotherapy, and experimentally validated interaction terms while maintaining the simplicity of low-dimensional models of tumor-immune interaction. In order to make useful suggestions about potential treatment plans, we require our model to meet reasonable biological assumptions. With appropriate parameter values, we expect to observe

- Uncontrolled growth of tumor cells in the absence of immune response,
- Immune cells reduce the number of tumor cells,
- Both immune cells and tumor cells decrease under chemotherapy.

In addition, we want the model to reflect that additional immune cells are activated and recruited by interactions between cancer cells and immune cells. The activation of tumor-killing cytotoxic T-cells is dependent on interactions between surface molecules on the T-cell and a tumor cell. Once activated, a T-cell undergoes clonal expansion, increasing the number of cells specific for the target antigen that can then travel throughout the body in search of antigen-positive tumor cells (Harlin et al. 2009; Smith-Garvin et al. 2009). Additional T-cells may also be activated by fragments of tumor cells that have been lysed by other cells (Huang et al. 1994).

The model should also reflect the results of CAR T-cell therapy studies, which have observed that sufficient lymphodepletion is an important factor in determining a durable response to treatment (Kochenderfer et al. 2017). We expect there to be some level of competition between endogenous effector cells and CAR T-cells, because both rely on cytokines such as interleukin 7 (IL7) and IL15, to proliferate (Rosenberg et al. 2008).

Finally, we want our model to reflect that immune cells can become inactivated through repeated interaction with tumor cells. Upon repeated exposure to tumor cells some T-cells experience exhaustion, an altered functional state in which they cannot effectively attack foreign cells (Thommen and Schumacher 2018).

We started from Kuznetsov's model, which includes only one group of activated immune cells or "effector" cells rather than multiple subpopulations of endogenous immune cells (Kuznetsov et al. 1994). Kuznetsov's model is

$$\frac{\mathrm{d}T}{\mathrm{d}t} = aT(1 - bT) - dET, \tag{1a}$$

$$\frac{\mathrm{d}E}{\mathrm{d}t} = g - mE + jE\frac{T}{k + T} - qET, \tag{1b}$$

where $T(t)$ is the population of tumor cells at time t and $E(t)$ is the population of effector cells at time t. For our model, we introduce a third equation to model the population of CAR T-cells and a fourth equation to model the concentration of chemotherapy. By including time-dependent source terms in these equations, we will be able to test treatment plans combining different CAR T-cell doses and lymphodepleting chemotherapy regimens. We also replace the second term in Eq. (1a) and the third term in Eq. (1b)

with experimentally validated, ratio-dependent interaction terms which de Pillis et al. (2005) demonstrated achieve a better fit to experimental data from cytotoxicity assays compared to simpler, classical choices such as mass action or Michaelis–Menten (which are used in the Kusnetsov model). We chose to adopt their novel interaction terms into the Kuznetsov model, rather than working with de Pillis et al.'s 5-equation model system, in order to focus on the minimal set of equations that would produce desired biological behaviors.

At time t, let $T(t)$ be the number of tumor cells, $E(t)$ be the number of endogenous effector cells, $C(t)$ be the number of CAR T-cells, and $M(t)$ be the concentration of a chemotherapy drug. The model system with treatment is

$$\frac{\mathrm{d}T}{\mathrm{d}t} = aT(1-bT) - D_E - D_C - K_T(1-e^{-M})T \tag{2a}$$

$$\frac{\mathrm{d}E}{\mathrm{d}t} = g - m_E E - j_E \ln\left(\frac{E+C}{K}\right)\frac{D_E^2}{k+D_E^2}E - q_E ET - K_E(1-e^{-M})E \tag{2b}$$

$$\frac{\mathrm{d}C}{\mathrm{d}t} = v_C(t) - m_C C - j_C \ln\left(\frac{E+C}{K}\right)\frac{D_C^2}{k+D_C^2}C - q_C CT - K_C(1-e^{-M})C \tag{2c}$$

$$\frac{\mathrm{d}M}{\mathrm{d}t} = v_M(t) - \gamma\, M \tag{2d}$$

where

$$D_E = d_E\frac{(E/T)^l}{s+(E/T)^l}T \quad \text{and} \quad D_C = d_C\frac{(C/T)^l}{s+(C/T)^l}T. \tag{3}$$

In the absence of treatment and effector cells, tumor cells grow logistically towards a carrying capacity of b^{-1}. In the absence of tumor cells, effector cells are produced at a fixed rate, g, and decay at a rate proportional to the population, $m_E E$.

Endogenous effector cells and CAR T-cells kill tumor cells according to a ratio-dependent tumor cell death term, D_E and D_C respectively, proposed by de Pillis et al. (2005). Numerous studies indicate that percent cell lysis is a function of the ratio of effector immune cells to tumor cells (Wang et al. 2019; Yang et al. 2006). In modeling the anti-tumor activity of $CD8^+$T-cells, de Pillis et al. (2005) considered the behavior of cells with a range of antitumor activity, from non-transduced cells, which have not been exposed to a target antigen and thus only mount a non-specific immune response, to primed $CD8^+$T-cells which have previously been exposed to the target antigen and mount a highly effective immune response. The authors found that the more effective the immune cells are at lysing their target cells, the more they follow a rational law dynamic. They speculated that this is because the highly effective cells operate closer to the saturation regime than other types of immune cells. Because we are modeling adoptive cellular therapies, which have shown very high anti-tumor activity (Kalos et al. 2011; Wang et al. 2019), this is an important model feature. For further exploration of the tumor cell lysis rate and how associated model parameters impact trajectories please see "Appendix C".

Effector cells and CAR T-cells are both recruited at a rate dependent on tumor cell lysis through a modified Michaelis–Menten term, $j_E D_E^2 E/(k + D_E^2)$ and $j_C D_C^2 C/(k + D_C^2)$ respectively. This recruitment term is then scaled by a competition factor $-\ln((E + C)/K)$, which limits the proliferation of immune cells when the size of the combined immune population approaches the carrying capacity, K. This competition factor, adopted from a CAR T-cell therapy model proposed by Kimmel et al. (2019), reflects the fact that there is a limited amount of immunological "space" which effector cells can occupy. The inactivation of immune cells upon exposure to tumor cells is incorporated through mass-action terms, $q_E ET$ and $q_C CT$, capturing the phenomenon of immune-cell exhaustion (Thommen and Schumacher 2018). Model parameters are defined in Table 1, and for details of parameter selection, please refer to "Appendix B."

We have incorporated CAR T-cell therapy into the model by including a governing equation for the engineered cell population (Kimmel et al. 2019; Sahoo et al. 2020). The dynamics for the CAR T-cell population consist of the same functional forms as the endogenous effector cells except that, instead of a constant source term, CAR T-cell injections of dose level P are modeled as a one-time increase in the number of engineered effector cells, $v_C(t)$, where

$$v_C(t) = \begin{cases} 0 & \text{if } t \neq \text{injection time} \\ \text{P} & \text{if } t = \text{injection time.} \end{cases} \tag{4}$$

By separating the dynamics of the endogenous effector cells from the engineered CAR T-cells, we are able to use different parameter values to define each population and incorporate competition between the two types of cells, creating a flexible framework to consider different adoptive cellular therapies.

Following the method of de Pillis et al. (2006), we also introduced a governing equation for the chemotherapy drug concentration. Here, γ is the decay rate of chemotherapy and $v_M(t)$ is a time-dependent forcing term encoding the dose strength, S (μM/day). The dosing schedule is

$$v_M(t) = \begin{cases} 0 & \text{if } t \notin \text{injection times} \\ \text{S} & \text{if } t \in \text{injection times} \end{cases} \tag{5}$$

where the injection times are the times during which a patient is receiving an infusion of chemotherapy. In the case of lymphodepleting chemotherapy, we are modeling regimens in which patients receive a uniform dose of chemotherapy over the course of one half hour each day for several days in a row. Consequently, $v_M(t)$ takes on the form of a collection of hat functions located at the start of each infusion period with height equal to the dose strength and width equal to one half hour. Elsewhere, $v_M(t)$ is uniformly zero.

We model the impact of chemotherapy by introducing saturating fractional cell-kill terms, $K_T(1 - e^{-M})T$, $K_E(1 - e^{-M})E$, and $K_C(1 - e^{-M})C$, to the equations for each cell population in Sys. (2a-c), again following the method of de Pillis et al. (2006). These expressions are nearly linear for low concentrations of chemotherapy

drug, $M(t)$, but the kill rate rapidly plateaus to the parameters K_T, K_E and K_C, respectively, as the concentration increases. This functional form has been shown to match dose-response curves from the literature (Gardner 2000). Note that different types of chemotherapy can be considered by varying the associated parameters: γ, K_T, K_E, and K_C.

3 Results

3.1 Model Behavior

In clinical practice, preconditioning chemotherapy is administered over a short time period, typically 3–5 days, followed by 2–14 days of rest, after which a single CAR T-cell injection is administered. Thus, in clinically relevant scenarios, the chemotherapy concentration $M(t)$ will decay fairly rapidly to zero, which is the only chemotherapy concentration steady-state relevant to our setting. Thus, when discussing the stability of the model given by Sys. (2), we assume that $M(t) = 0$ and focus our analysis on the first three equations, which govern the dynamics of the tumor, effector, and CAR T-cell populations. The details of analyzing this three-dimensional system (6) are given in "Appendix A." In particular, we scale the tumor cell count by the tumor carrying capacity, yielding $x = bT$, and we scale the immune cell populations by the ratio between the intrinsic effector cell growth rate and the tumor cell growth rate, yielding $y = aE/g$ and $z = aC/g$, to nondimensionalize Sys. (6) before proceeding with linear stability analysis.

We show analytically that for a wide range of biologically relevant parameters, Sys. (6) has at least two stable equilibria, both of which reside in the $C = 0$ plane, a zero-tumor (or tumor-free) equilibrium occurs at the point ($T = 0$, $E = g/m_E$, $C = 0$) and a high-tumor equilibrium occurs where the tumor cell population is near the carrying capacity. Nullsurfaces and equilibria of the nondimensionalized system (Sys. (8)) in the plane $z = 0$ are plotted in Fig. 1a for the Patient 3 parameter set (column 5 of Table 1). The tumor-free equilibrium is at the point ($x = 0$, $y = 1/m_y$, $z = 0$) and the high-tumor equilibrium is at the point ($x \approx 1$, $y \approx 1/(q_y + m_y)$, $z = 0$). We also determined numerically that as shown in Fig. 1a, there is a saddle point for a relatively small number of tumor and effector cells. Note that in Fig. 1a, b, we are only plotting the positive quadrant because it is an invariant set for this system. Thus, if we start with a nonnegative initial condition, the model will never predict a negative population of cells, a desired property for biological interpretability.

We numerically located and assessed the stability of interior equilibria of the nondimensionalized system (8) as well (Fig. 1b). For the parameter sets considered here (listed in Table 1 and described in Sect. 3.2.2, with further details in "Appendix B"), there is a saddle point located at a moderate tumor cell population, low effector cell population, and high CAR T-cell population. This saddle point significantly shapes trajectories, causing non-monotonic behavior, notably pseudo-progression of the tumor whereby the tumor initially increases after CAR T-cell treatment before ultimately being eradicated. The stable manifold of this saddle point separates the basin of attraction for healthy outcomes from the basin of attraction for unhealthy outcomes. There

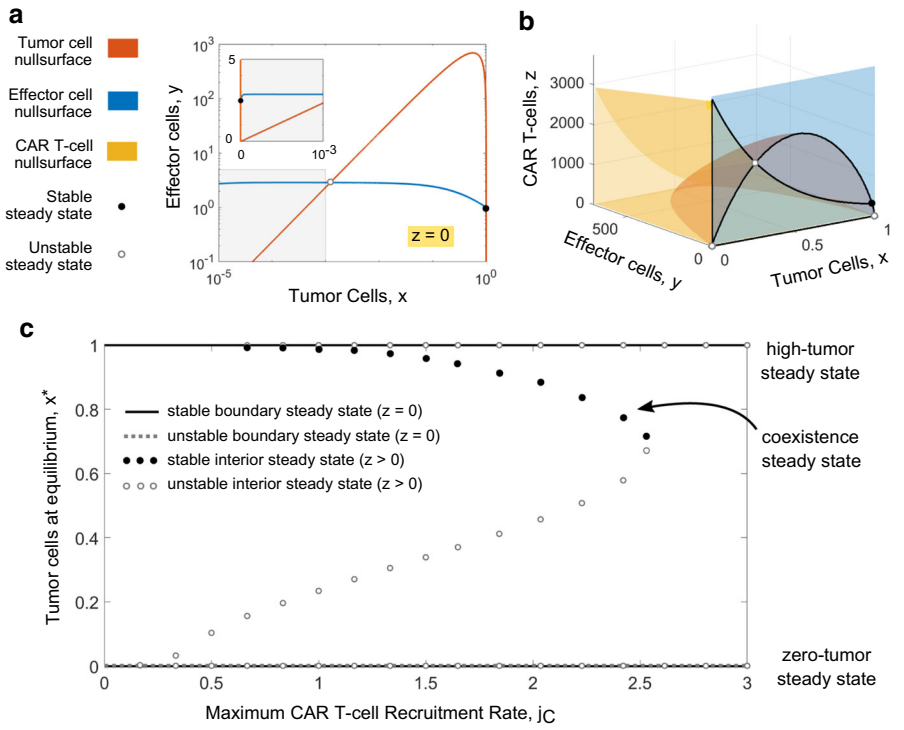

Fig. 1 Nullsurfaces and equilibria for the nondimensionalized system (8) are shown for the Patient 3 parameters (column 5 of Table 1). The nondimensional state variables are $x = bT$, $y = aE/g$, and $z = aC/g$. **a** Boundary equilibria lie at the intersections of the effector and tumor cell nullsurfaces on the CAR T-cell nullsurface $z = 0$, plotted here. For a wide range of parameters, there are two stable equilibria (solid circles) and a saddle point (open circle). **b** Interior steady states lie at the intersections of the nonzero nullsurfaces for the tumor, effector, and CAR T-cell populations. Intersections between the effector cell nullsurface and the nullsurfaces for the other two cell populations are emphasized with black lines. For this set of parameters, there is one stable interior equilibrium (solid circle). There are three unstable interior steady states indicated by open circles: an unstable node near the origin, a saddle point at a high number of CAR T-cells and moderate tumor cell count, and another saddle point at x just less than 1 and a very small number of CAR T-cells. **c** Bifurcation diagram created by varying the maximum CAR T-cell recruitment rate, j_C, while fixing all other parameters at their Patient 3 value. For each value of j_C, the tumor cell counts, x^*, of all existing equilibria were computed numerically. The three boundary equilibria that lie in the $z = 0$ plane (shown in **a**) remain constant for all values of j_C, and are denoted by solid lines (stable) and a dashed line (unstable) in panel **c**. As j_C changes, interior equilibria appear and disappear in a sequence of 3 saddle node bifurcations. Unstable interior equilibria are marked by open gray circles and the stable interior equilibrium, referred to as the coexistence state, is marked by black circles

is an additional unstable interior equilibrium at a low population level for all three cell types which contributes to the spike in CAR T-cell populations seen in healthy trajectories before the CAR T-cell population starts declining.

For the Patient 1 and 2 parameters sets given in Table 1, only the two interior equilibria mentioned above exist. However, for some parameter values, including Patients 3 and 4 from Table 1, two additional equilibria appear near the high-tumor equilibrium. One is a stable node, which we refer to as the coexistence equilibrium

Table 1 Parameter values used in numerical simulations

Parameter	Description	Patient 1	Patient 2	Patient 3	Patient 4
a	Tumor growth rate (day^{-1})	2.55e−1	1.76e−1	5.14e−1	5.14e−1
$1/b$	Tumor carrying capacity (cells)	2e12	2e12	9.804e8	9.804e8
d_E	Saturation level of tumor kill by effector cells (day^{-1})	2.03	2.03	5.8	4.23
d_C	Saturation level of tumor kill by CAR T-cells (day^{-1})	2.25	2.25	2.25	2.25
g	Base recruitment rate of effector cells (cells/day)	1.4e3	4.7e4	1.3e4	1.3e4
j_E	Max recruitment rate of effector cells by tumor lysis (day^{-1})	1.1e−2	7.46e−3	2.7e−2	2.7e−2
j_C	Max recruitment rate of CAR T-cells by tumor lysis (day^{-1})	2.42e−1	1.65e−1	6.0e−1	6.0e−1
K	Effector cell carrying capacity (cells)	1.65e9	1.65e9	1.65e8	1.65e8
k	Steepness of effector cell recruitment curve ($cells^2 day^{-2}$)	2.019e5	7.0e7	2.0e7	2.0e7
l	Exponent of tumor lysis by effector cells (unit-less)	1.395	1.419	1.36	1.43
m_E	Effector cell death rate (day^{-1})	7e−3	3.4e−2	2e−2	2e−2
m_C	CAR T-cell death rate (day^{-1})	2.93e−2	2.93e−2	2.93e−2	2.93e−2
q_E	Effector cell inactivation by tumor ($cells^{-1} day^{-1}$)	3.42e−11	6.716e−11	3.42e−10	3.42e−10
q_C	CAR T-cell inactivation by tumor ($cells^{-1} day^{-1}$)	3.0e−11	3.0e−11	1.53e−9	1.53e−9
s	Steepness of fractional tumor cell kill by effector cells (unit-less)	3.05e−1	3.05e−1	2.5e−1	3.6e−1
K_T	Fractional tumor cell kill by chemotherapy (day^{-1})				7.00e−1
K_E, K_C	Fractional healthy cell kill by chemotherapy (day^{-1})				6.00e−1
γ	Chemotherapy decay rate (day^{-1})				9.00e−1

Parameter values from ranges for large B-cell lymphoma reported by Rösch et al. (2016) were selected for Patient 1. Parameter values from ranges for B cell Chronic Lymphocytic Leukemia reported by Nanda et al. (2013) were selected for Patient 2. The Patient 3 and 4 parameter values come from two metastatic melanoma patients, reported by de Pillis et al. (2005). CAR T-cell related parameters are adapted from Kimmel et al. (2019)

because all 3 cell populations persist at nonzero levels. Due to the fact that the tumor burden remains at around 95% of the high-tumor value, trajectories that approach this steady state are also considered an unhealthy outcome. The other equilibrium that appears is a third saddle point, with the stable manifold now separating trajectories that approach the high-tumor equilibrium from those that approach the coexistence equilibrium.

Changing the parameter values characterizing CAR T-cells causes interior equilibria to appear and disappear. The maximum CAR T-cell recruitment rate, j_C, can be tuned to observe the sequence of saddle node bifurcations creating and destroying the interior equilibria (Fig. 1c). When $j_C = 0$, the only CAR T-cell nullsurface is the plane $C = 0$, and there are no interior equilibria. For small values of j_C, an unstable node and saddle point appear near the origin. As j_C increases, the saddle point moves higher (in an x-axis and z-axis sense) along the tumor-cell null surface, allowing larger spikes in CAR T-cells to occur for trajectories that ultimately reach the high-tumor outcome. Patient parameter sets 1 and 2 lie in this regime. Increasing j_C still further pushes the system past a critical threshold in which the recruitment of CAR T-cells in response to the high tumor burden balances the natural death and deactivation rate of CAR T-cells, so the CAR T-cell population is able to persist for some initial conditions. Patient parameter sets 3 and 4 lie in this regime, in which the stable coexistence equilibrium has appeared simultaneously with a saddle point near the high tumor equilibrium. As j_C continues to increase, the coexistence equilibrium shifts to lower and lower tumor values, and the saddle point causing spikes in the CAR T-cell population shifts to higher tumor values. Eventually, the two collide and disappear, leaving three unstable interior equilibria. The equilibria in the $C = 0$ plane remain unchanged throughout because they are independent of j_C.

3.2 Evaluation of Treatment Plans

Standard treatment protocols incorporate a lymphodepleting preconditioning regimen which consists of a round of chemotherapy prior to CAR T-cell infusion. We tested realistic combinations of chemotherapy preconditioning and CAR T-cell doses by simulating treatment plans with parameter sets from several different cancer types using Sys. (2) and evaluating the outcomes. Here, we discuss the scenarios considered and simulation results.

3.2.1 Treatment Plans Considered

We explored combinations of chemotherapy preconditioning and CAR T-cell doses from a range that encompasses the standard procedures for the two FDA approved CAR T-cell treatments, Yescarta (Kite 2017) and Kymriah (Novartis 2017). The guidelines for dosing CAR T-cells prescribe $0.2 - 5.0 \times 10^6$ cells per kilogram of body weight up to a maximum of 2.5×10^8 cells (Kite 2017) or 6×10^8 cells (Novartis 2017). We consider injections of $P = 1 \times 10^7$ cells, $P = 1 \times 10^8$ cells, and $P = 2.5 \times 10^8$ cells referred to as dose level 1 (DL1), dose level 2 (DL2), and dose level 3 (DL3) respectively. However, studies have shown that only a small fraction of injected CAR

T-cells remain in circulation in the blood (Turtle et al. 2016). To reflect this in our numerical simulations, we scaled down the effective dose, P, to be 1% of the injected dose level (Turtle et al. 2016).

The standard chemotherapeutic preconditioning regimen for both drugs is a combination of fludarabine and cyclophosphamide administered over three to five days. We considered two chemotherapy regimens, either medium strength for one half hour each day for 5 days (C5), or high strength for one half hour each day for 3 days (C3). The strengths were chosen so that the peak concentration of chemotherapy during the five-day regimen matched the value reported in a pharmacokinetic study of fludarabine (Ju et al. 2014), and the overall exposure in the two plans was equal (measured by the area under the chemotherapy concentration curve). In practice, lymphodepletion is followed by either a three-day rest period for Yescarta (Kite 2017) or 2–14 days rest for Kymriah (Novartis 2017) before T-cell injection. For all combinations, we started by enforcing the minimum rest period of 2 days between the end of chemotherapy and the T-cell injection.

3.2.2 Patients

We considered four parameter sets in our evaluation, each representing a different theoretical "patient". The first patient constitutes typical parameter values for diffuse large B-cell lymphoma (Rösch et al. 2016). Rösch et al. estimated a range of model parameters using data from randomized clinical trials in elderly patients. Our second patient parameter set is drawn from typical parameter values for B-cell chronic lymphocytic leukemia (Nanda et al. 2013). Nanda et al. analyzed existing data in the medical literature to determine ranges of values for model parameters and calibrated their model to clinical patient data. Currently, CAR T-cell therapy has been approved for use with several blood cancers; however, numerous clinical trials are testing its potential for treatment of solid cancers as well, including melanoma (Brown and Mackall 2019; Zhang et al. 2014). De Pillis et al. (2005) used data from two metastatic melanoma patients reported in a clinical trial to fit their model for mixed chemotherapy and immunotherapy treatment. We use their resulting parameter values for our last two patient parameter sets. The model assumptions are predicated on CAR T-cells effectively targeting tumor cells. Hence, simulation results suggest possible outcomes once good target antigens have been identified for metastatic melanoma. Parameters characterizing the CAR T-cell population were adapted from a model put forward by Kimmel et al. (2019). Their model parameters were fit to data from the ZUMA-1 clinical trial of CAR T-cell therapy for adults with refractory aggressive Non-Hodgkin Lymphoma. The parameters we used for Patient 1–4 are listed in Table 1, and the details of parameter selection are discussed in "Appendix B."

Given a set of patient parameters, partitioning the phase space into basins of attraction for the healthy versus unhealthy outcomes provides intuition into how that patient will respond to treatment. Basins of attraction computed using the three-equation model (Sys. (8)), which governs the dynamics of the tumor, effector, and CAR T-cell populations, are illustrated for Patients 1 and 3 in Fig. 2. Panels a–b show an ensemble of initial conditions which have been treated with 3 days of high-strength chemotherapy and 10^7 CAR T-cells, with 4 days of rest in between. The trajectories shown in Fig.

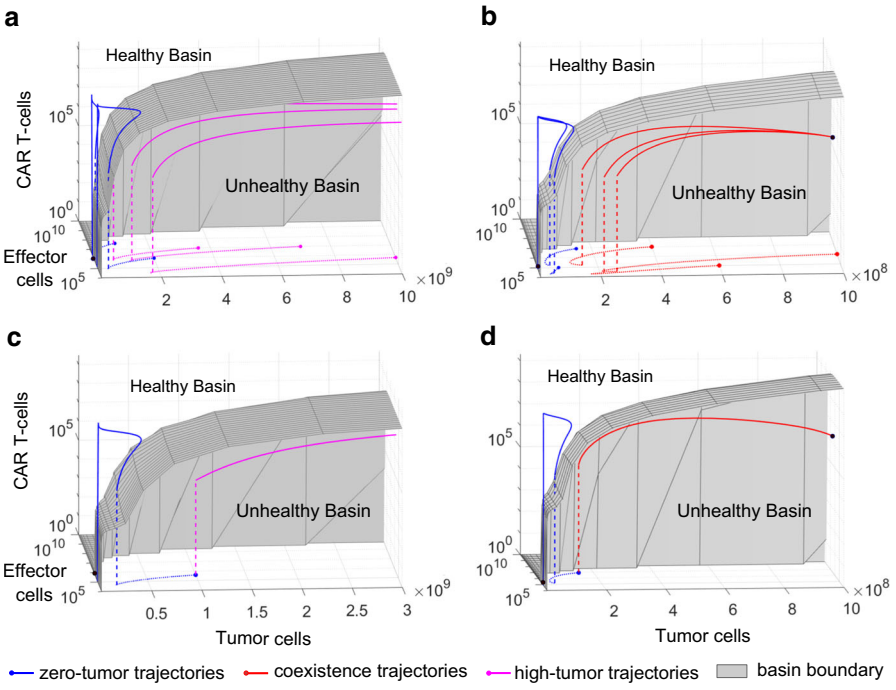

Fig. 2 Combination treatment trajectories in a three-dimensional view of phase space showing the tumor, effector, and CAR T-cells. The surface separating the basin of attraction for the healthy zero-tumor steady state from the basin of attraction for unhealthy outcomes is shown in gray (computed numerically for Sys. (6)). Example trajectories in which the initial condition was treated with chemotherapy at strength $S = 125$ for one half-hour each day for 3 days, followed by 4 days of rest before a CAR T-cell dose of 10^7 cells were simulated for **a** Patient 1 (column 3 of Table 1) and **b** Patient 3 (column 5 of Table 1) using Sys. (2). The dotted portion of each trajectory precedes CAR T-cell injection and thus is confined to the plane $C = 0$. The dashed vertical line shows the CAR T-cell dose administered. After this injection, if the patient condition lies above the surface it will ultimately approach the healthy zero-tumor outcome (blue trajectories), but if the patient condition is still below the surface it will approach an unhealthy patient outcome. The magenta trajectories in panel **a** approach the high-tumor equilibrium beyond the edge of the plot at the point $(T^* = 2 \times 10^{12}, E^* = 2.05 \times 10, C^* = 0)$, and the red trajectories in panel **b** approach the coexistence equilibrium. In both patients, successful CAR T-cell treatments result in higher, more prominent CAR T-cell peaks compared to unsuccessful treatments. In the patient scenarios shown in **c** (Patient 1) and **d** (Patient 3), when a dose of 10^7 CAR T-cells is administered at the patient initial condition (blue dot), CAR T-cells expand post injection, but the tumor progresses monotonically toward an unhealthy equilibrium—the high-tumor steady state beyond the edge of the plot in the case of Patient 1 and the coexistence equilibrium in the case of Patient 3. However, under the chemotherapeutic preconditioning described above, the patient condition is shifted to a lower tumor and effector cell burden prior to CAR T-cell injection. From this preconditioned state, the same CAR T-cell dose of 10^7 cells now succeeds at shifting both patients to the healthy basin of attraction

2a, b would all approach an unhealthy outcome in the absence of treatment, illustrated by the fact that the initial conditions lie within the unhealthy basin (region below gray surface). For moderate-to-large tumors, the CAR T-cell dose necessary to move the patient condition to the healthy basin of attraction (region above gray surface) scales with the tumor burden, rapidly climbing to medically infeasible levels. However, as illustrated by the dashed portion of trajectories, chemotherapeutic preconditioning shifts initial conditions toward the origin, reducing tumor burden and lowering the number of effector cells potentially competing with injected CAR T-cells. For some conditions, this shift is sufficient to allow medically feasible injections of CAR T-cells to proliferate and eradicate the tumor, but if a trajectory is still in the unhealthy basin of attraction for a given patient after both chemotherapy and CAR T-cell injection, that treatment plan will not be effective. In these cases, after tumor regression under chemotherapy, the tumor progresses again. Panels c and d of Fig. 2 highlight outcomes from a single initial condition for each patient. Without preconditioning, the CAR T-cell dose does not lift the condition out of the unhealthy basin of attraction, and the tumor burden grows toward either the high-tumor steady state (Patient 1 in Fig. 2c) or the coexistence state (Patient 3 in Fig. 2d). However, with preconditioning, the CAR T-cell dose succeeds for both patients, and the trajectory approaches the healthy zero-tumor steady state. We observe that the successful CAR T-cell trajectories reach a higher, sharper CAR T-cell peak than the unsuccessful trajectories (Fig. 2).

The initial conditions tested for each patient cover a range of tumor magnitudes. For Patient 3 and 4 the minimum value is close to the smallest detectable tumor size, and the maximum is the carrying capacity for tumor cells in the absence of effector cells. The values considered were a low tumor burden (low TB) at 1×10^8 tumor cells, medium tumor burden (medium TB) at 5×10^8 tumor cells, and high tumor burden (high TB) at 9.8×10^8 tumor cells (de Pillis et al. 2006). For Patient 1 and 2, we tested initial conditions an order of magnitude higher to reflect the higher tumor cell carrying capacity. The values considered for Patients 1–2 were a low tumor burden (low TB) at 1×10^9 tumor cells, medium tumor burden (medium TB) at 5×10^9 tumor cells, and high tumor burden (high TB) at 1×10^{10} tumor cells. The initial number of effector cells was set to 4×10^5 cells, which is the average of the zero-tumor equilibrium values for all four patient parameter sets (Rösch et al. 2016). The estimated average number of T-cells activated against a given antigen is higher; however, cancer cells are notoriously hard for the immune system to recognize, so it is reasonable to consider a smaller initial immune response (Pandya et al. 2016).

3.2.3 Single Treatment Plan Outcomes

First, we tested the CAR T-cell doses and lymphodepleting regimens one at a time to verify the impact on each tumor burden. In all scenarios, lymphodepleting chemotherapy alone initially reduced the tumor burden and endogenous immune cells, but ultimately resulted in tumor progression. CAR T-cell injection without prior lymphodepletion also failed in all scenarios. When the endogenous effector cell population is high, even at a moderate tumor burden, the CAR T-cell population is unable to mount an effective response due to competition from the endogenous cells. Generally, the dosage of CAR T-cells necessary to treat a patient initial condition without precondi-

tioning lies well beyond the maximum dosage deemed safe, unless the initial tumor burden is very small. This limitation drives the need to combine these two treatment modalities in order to effectively combat cancer.

3.2.4 Combination Treatment Plan Outcomes

After testing single-modality treatments, we considered combination treatments. In Fig. 3, we illustrate a range of possible patient trajectories from numerical simulations of combination treatment for Patients 1–4 at medium tumor burden. The effect of the three-day high strength chemotherapy plan, followed by 4 days of rest before a CAR T-cell injection at DL3 is shown for Patients 1 and 2 (Fig. 3a–c). In both cases, the system would have monotonically progressed to the high-tumor steady state without intervention. Under this combined treatment plan, tumor cells initially decrease during chemotherapy for both patients, but then progress again when chemotherapy stops. After CAR T-cell injection, the CAR T-cell population increases. For Patient 1, the CAR T-cell expansion is not sufficient to reverse tumor progression and, as the tumor continues to grow, eventually the immune cells become exhausted and the CAR T-cell population is driven down to zero. However, for Patient 2, though the tumor initially progresses after CAR T-cell injection, the engineered cells expand enough to reverse tumor growth and eliminate the tumor around 30 days after injection. Once the tumor is eliminated, the CAR T-cell population gradually declines and the endogenous effector cell population continues to recover from a post-chemotherapy low. The effect of the five-day medium-strength chemotherapy plan, followed by 2 days of rest before a CAR T-cell injection at DL2 is shown for Patients 3 and 4 (Fig. 3d–f). Again, for both patients the system would have rapidly progressed to the high-tumor steady state without intervention. Similarly to Patients 1 and 2, during preconditioning, the tumor initially decreases, but then progresses once chemotherapy stops, and the CAR T-cell population increases immediately following injection. In the case of Patient 3, CAR T-cells peak at 12 days, but after this point the cell populations converge to their coexistence values, which involves an unsustainable tumor burden and is thus an unsuccessful patient outcome. In Patient 4, however, CAR T-cells expand sufficiently well to reverse initial pseudo-progression of the tumor and eliminate tumor cells around 18 days after CAR T-cell injection. Again, when the tumor is eliminated, the CAR T-cell population gradually declines and the endogenous effector cell population recovers.

Figure 4 summarizes the outcomes of combination treatments for all theoretical patient scenarios. Notably, for all patients, we observe conditions that cannot be treated by medically feasible CAR T-cell injection alone, but are treatable with chemotherapy and CAR T-cell injection in combination. For the dose levels considered here, CAR T-cell injection and lymphodepleting chemotherapy were never effective for Patient 1 with high TB.

Between the fixed preconditioning regimens considered, the three-day high-strength and the five-day medium-strength chemotherapy dosing schedules often had similar outcomes. However, there are several cases in which preconditioning with the five-day plan results in successful treatment where the three-day plan fails. For example, in Patient 1 medium TB, combining five-day chemotherapy with DL1 was

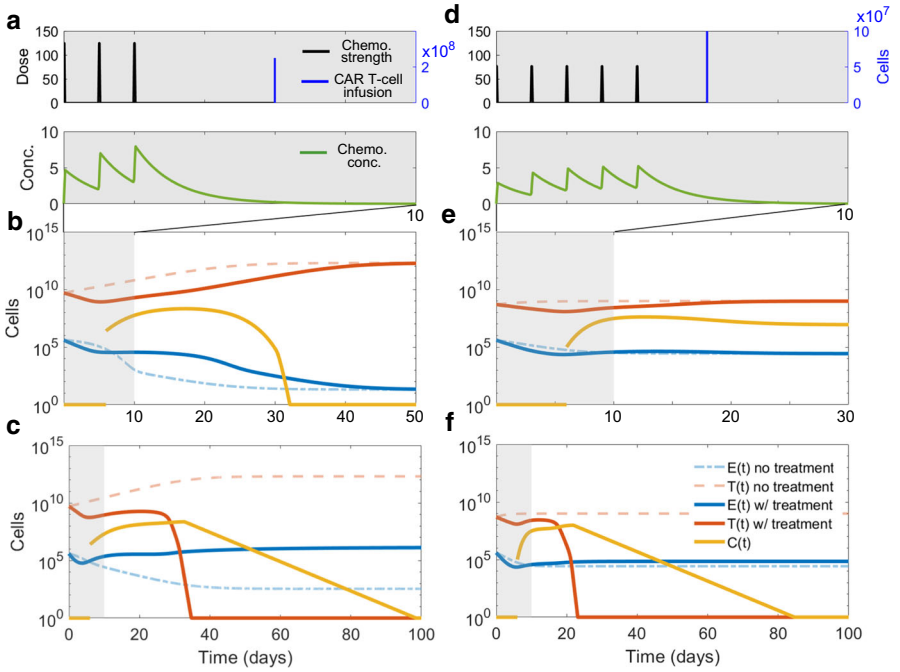

Fig. 3 Example combination treatments in four patients simulated using Sys. (2). In all cases, the system without treatment (no chemotherapy or CAR T-cell dose) would approach the high-tumor steady state. Combining the three-day high-strength chemotherapy plan with a four-day rest period and an injection of DL3 $= 2.5 \times 10^8$ CAR T-cells illustrated in **a** produces an unsuccessful outcome for **b** Patient 1, but succeeds for **c** Patient 2. Combining the five-day medium strength chemotherapy plan with a 2-day rest period and an injection of DL1 $= 10^7$ CAR T-cells illustrated in **d** produces a successful outcome for **e** Patient 3, but an unsuccessful outcome for **f** Patient 4. The first 10 days are shaded gray in each plot to show when treatment is being applied

	C3-DL1	C3-DL 2	C3-DL3	C5-DL1	C5-DL2	C5-DL3
P1: Low TB	7	9	9	9	10	11
P1: Med TB	x	2	3	2	4	4
P1: High TB	x	x	x	x	x	x
P2: Low TB	10	12	13	13	15	17
P2: Med TB	x	2	4	4	6	7
P2: High TB	x	x	x	x	x	3
P3: Low TB	3	3	4	3	3	4
P3: Med TB	x	2	3	x	2	2
P3: High TB	x	x	x	x	x	2
P4: Low TB	3	4	4	3	4	4
P4: Med TB	x	2	3	2	2	3
P4: High TB	x	x	2	x	2	2

Maximum rest period:
> 15 days
10-15 days
5-10 days
3-5 days
2 days
unsuccessful

Fig. 4 Maximum number of rest days between indicated chemotherapy plan and CAR T-cell dose resulting in a successful treatment outcome for three initial conditions based on numerical simulations using the parameter sets for Patients 1–4 recorded according to the following key: DL1 = 1×10^7 cells, DL2 = 1×10^8 cells, DL3 = 2.5×10^8 cells, C3 is 3 days of chemotherapy at high strength, C5 is 5 days of chemotherapy at medium strength. Treatment combinations that failed even with the minimum rest period of 2 days are shaded red and indicated by an x

effective in eliminating the tumor, but combining three-day chemotherapy with the same dose of CAR T-cells was not. The same result occurs for Patient 2 medium TB and DL1, Patient 2 high TB and DL3, Patient 3 high TB and DL3, Patient 4 medium TB DL1, and Patient 4 high TB DL2. Plots of the time course of the trajectories under these two treatment plans for Patient 1 medium TB are shown in Fig. 5. Without treatment, the tumor-cell count climbs toward the carrying capacity and the effector-cell count drops, approaching the high-tumor equilibrium. Introducing 3 days of high-strength chemotherapy reduces the tumor burden, but when chemotherapy ends and the CAR T-cell injection is administered on day 5, the tumor progresses toward its carrying capacity despite an initial increase in the CAR T-cell population, which ultimately drops to zero (Fig. 5a). In contrast, 5 days of medium-strength chemotherapy reduces the tumor burden and endogenous effector cell population enough so that after CAR T-cell injection on day 7, the engineered cells climb to a higher and later peak. Initially, the tumor progresses, but around day 20 the tumor-cell count begins to steadily decline to zero. Once the tumor burden is reduced, the CAR T-cell population begins to decline, while the endogenous effector cells slowly recover (Fig. 5b). Although the area under the chemotherapy concentration curve is the same in these two scenarios, spreading the concentration over 5 days instead of 3 dramatically changes the patient's outcome. The tumor and effector cell counts on day 3 of the high-strength plan are lower than the cell counts on day 3 of the medium-strength plan. However, the doses are high enough that the advantage of the higher dose in the 3-day high strength plan is only slight and does not compensate for the longer exposure of the 5-day medium strength plan. The advantage of the 5-day plan then holds throughout the subsequent rest period and causes the difference in post-CAR T-cell injection outcomes. The difference between the kill rates for the two plans is small due to the saturating nature of the chemotherapy cell kill term, a property which has been widely supported in the literature (de Pillis et al. 2006; Gardner 2000; Pinho et al. 2002; Ribba et al. 2012).

Finally, our simulations showed that the rest period between the end of preconditioning and T-cell injection impacts patient outcome. For example, administering 5 days of high-strength chemotherapy, allowing 4 days of rest, and then administering an injection of CAR T-cells at DL3 is not an effective intervention for Patient 2 high TB (Fig. 6a). However, if the rest period is limited to 3 days instead of 4, the combination is successful (Fig. 6b). During the extended rest period, the tumor-cell count climbs high enough that a CAR T-cell injection that would be effective with a shorter rest period fails. For each combination of chemotherapy and CAR T-cell therapy that succeeded with a two-day rest period where the CAR T-cell dose alone failed, we determined the maximum possible rest period with which the combination was still effective (Fig. 4). Over 70% of these scenarios failed if the rest period was 5 days or greater. Nearly, 90% of the scenarios failed if the rest period was longer than 12 days. All of the scenarios failed if the rest period was longer than 17 days. This suggests that the length of the rest period between chemotherapeutic lymphodepletion and CAR T-cell injection can have important implications for patient outcome. As rest periods can range widely under current guidelines, from 2–14 days, this is an important aspect of treatment to investigate more thoroughly.

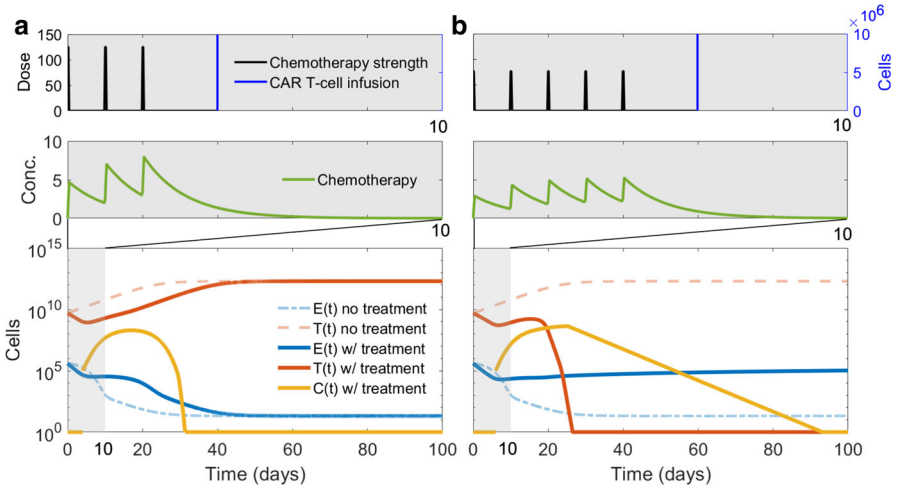

Fig. 5 Numerical simulations of treatment of medium TB for Patient 1. **a** Three days of high-strength chemotherapy are combined with a CAR T-cell injection of 1×10^7 cells, producing an unhealthy outcome. **b** The five-day medium strength chemotherapy plan is combined with the same CAR T- cell injection resulting in a successful patient outcome. The relevant treatment plan is illustrated in the panels above the cell population trajectories, and the first 10 days are shaded gray in all panels, emphasizing when treatment is occurring

3.3 Sensitivity Analysis

We performed a sensitivity analysis on the model proposed in Sys. (6) to identify which parameters have the largest impact on the effectiveness of CAR T-cell injections. For each patient, we calculated the precise dose of CAR T-cells necessary to shift the low-TB initial condition to a healthy patient outcome. We call this number of CAR T-cells, the CAR T-cell success threshold, because any treatment plan which injects a dose of CAR T-cells exceeding this quantity will be successful (in theory) against tumor burdens up to and including the low TB (Fig. 7a).

For the sensitivity analysis, we varied each parameter up and down by 1% while holding the other parameters constant and calculated the resulting change in the CAR T-cell success threshold. (See "Appendix C" for details of sensitivity analysis.) Across all patients, the exponent in the tumor-cell lysis rate, l, had the largest impact on the high-tumor threshold (Fig. 7b). A 1% change in l results in a 5–7% shift in the threshold, which indicates that small changes in the effectiveness of CAR T-cells against tumor cells will affect clinical outcomes. The tumor growth rate a had a significant impact on the threshold for all parameter sets, indicating that cancers characterized by a higher growth rate will require higher CAR T-cell doses for a given initial condition. Across the four patients, a 1% change in the maximum CAR T-cell recruitment rate, j_C, resulted in a $3-5\%$ change in the CAR T-cell success threshold, supporting the notion that improving the ability of CAR T-cells to expand can significantly lower the necessary number of injected cells.

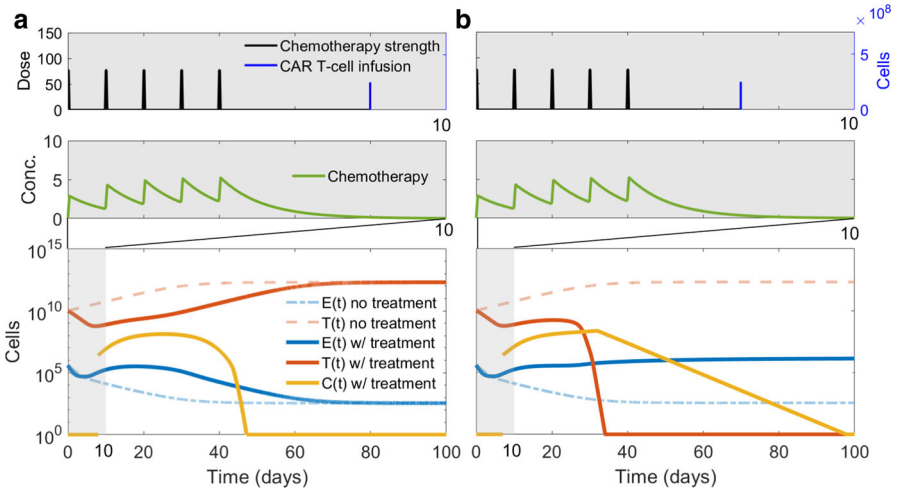

Fig. 6 **a** Combining five days of high-strength chemotherapy and 2×10^8 CAR T-cells sequentially with a four-day rest period in between allows the tumor to escape. **b** However, combining the two treatments with a three-day rest period results in tumor elimination and a healthy outcome. Both simulations were run using parameters from Patient 2 and assuming high TB. The relevant treatment plan is illustrated in the panels above the cell population trajectories, and the first 10 days are shaded gray in all panels to emphasize when treatment is occurring

Of the remaining parameters, those characterizing CAR T-cells had the largest impact on the CAR T-cell success threshold. The maximum tumor cell lysis rate by CAR T-cells, d_C, the death rate m_C, the deactivation rate by tumor cells q_C, the half-saturation value of tumor cell lysis, s, and the joint carrying capacity K all had a smaller, but non-negligible impact on the high-tumor threshold. Targeting these aspects of CAR T-cell function could be helpful. In contrast, changes in the parameters defining the steepness of the immune cell recruitment curves, k, and the remaining parameters defining effector cell dynamics, g, d_E, j_E, k_E, m_E and q_E, had little effect on the CAR T-cell success threshold.

De Pillis et al. performed a sensitivity analysis on their 2005 model, from which we adapted several interaction terms. They found that the tumor size at $t = 25$ days was most sensitive to the tumor growth rate a and the exponent in the tumor lysis rate, l. Our results confirm the importance of these two parameters even when measuring a different model feature.

4 Discussion and Conclusion

We have developed and analyzed a mathematical model consisting of a system of ordinary differential equations that can be used to test combinations of preconditioning chemotherapy regimens and CAR T-cell doses. We also found that under biologically relevant parameter values the system has at least two stable equilibrium points, one "healthy," tumor-free equilibrium and one "unhealthy," high-tumor equilibrium. Adjusting the parameters characterizing CAR T-cell interactions with tumor cells can

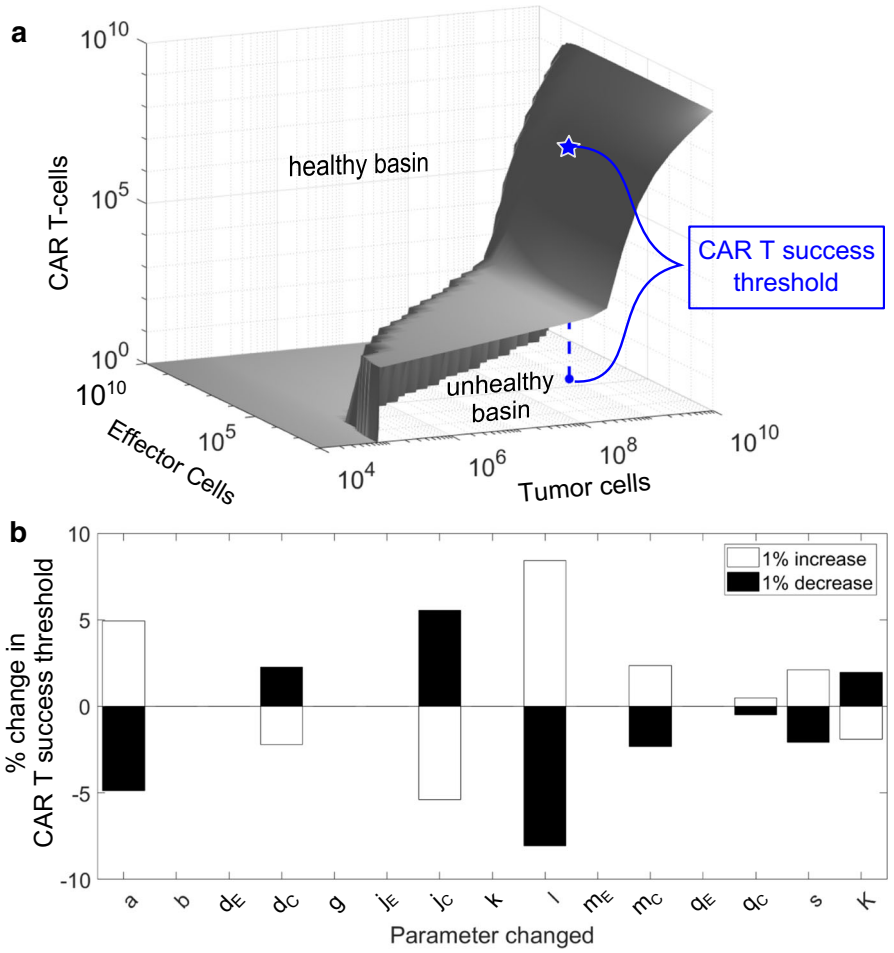

Fig. 7 **a** We define the CAR T-cell success threshold as the minimum number of CAR T-cells needed to contain the low-tumor burden without chemotherapy. **b** Here, sensitivity analysis shows that the CAR T success threshold is most sensitive to the tumor-cell lysis rate exponent (l) for Patient 1. The other model parameters tested are the tumor growth rate (a), the inverse of the tumor cell carrying capacity (b), the maximum tumor cell kill rate by endogenous effector cells (E cells) (d_E), the maximum tumor cell kill rate by CAR T-cells (d_C), the E cell growth rate (g), the maximum recruitment rate of E cells (j_E), the maximum recruitment rate of CAR T-cells, the half-saturation value of E cell proliferation, (k_E), the half-saturation of CAR T-cell proliferation (k_C), the E cell death rate (m_E), the CAR T-cell death rate (m_C), the E cell inactivation rate by tumor cells (q_E), the CAR T-cell inactivation rate by tumor cells (q_C), the half-saturation value of the tumor cell lysis rate (s), and the joint carrying capacity of E and CAR T-cells (K). Similar figures for the other patient parameter sets are included in "Appendix C"

also cause an "unhealthy," stable coexistence equilibrium to emerge. The basins of attraction for these equilibria were determined numerically. The variation between the shapes of the basins of attraction for different parameter sets reflect the fact that responses to treatment will not be uniform across patients.

We tested treatment plans that adhere to standard CAR T-cell therapy protocols on patient parameter sets from several cancer types. Our goal was not to propose any novel therapy plans or unrealistic dosing schedules, but rather to uncover refinements that are attainable within current practice and that merit additional attention. We observed a variety of outcomes supporting three main conclusions:

First, our model predicts that, without preconditioning, medically infeasible CAR T-cell injections would be required to successfully treat moderate to large tumor burdens. The necessary CAR T-cell dose can be quantified by characterizing the boundary between the basin of attraction for the healthy versus unhealthy equilibria for a patient parameter set. Successful preconditioning shifts a patient initial condition to lower tumor and endogenous effector cell counts where the boundary to reach the healthy basin of attraction is lower, and so safe levels of CAR T-cell therapy are effective (Fig. 7a). We have shown that CAR T-cell doses currently used in clinical practice are sufficient to move patient conditions to the healthy basin of attraction after preconditioning chemotherapy, resulting in a successful treatment outcome, in a significant proportion of patient scenarios. One model parameter closely associated with the height of the boundary between healthy and unhealthy patient outcomes is the exponent of the tumor-cell lysis rate, l, which relates to how effectively CAR T-cells kill tumor cells. This observation suggests that small changes in the effectiveness of CAR T-cells can have a large impact on the dosage required for successful adoptive cellular therapy.

Second, appropriate chemotherapeutic lymphodepletion can reduce the CAR T-cell dosage necessary for successful treatment. Lymphodepletion lowers the necessary dose of CAR T-cells through two modes: reducing the tumor burden, and reducing the endogenous effector cell population, thereby allowing the injected cells to expand. This was observed in treatment scenarios for all four patients considered. Lower tumor burden at the time of injection and lower CAR T-cell doses are associated with milder side effects, which implies that selecting the appropriate lymphodepletion plan can make CAR T-cell therapy safer.

Finally, the recovery period between the end of preconditioning chemotherapy and the administration of a CAR T-cell injection matters. If the recovery period is too long, the benefits of lymphodepletion may be lost. This finding in particular warrants further investigation as under current practice the rest period can vary from as low as 2 up to as high as 14 days. Notably, for the two patient parameter sets with large tumor growth rates, Patients 3 and 4, the maximum successful rest window was less than 5 days. According to our sensitivity analysis, the tumor growth rate, a, was also an influential factor determining the minimum CAR T-cell dose necessary for successful treatment. Ideally, model parameters could be tuned to match a patient's tumor growth rate in order to suggest how strictly the rest period should be limited.

The model proposed and explored here has several limitations. First, the choice of an ODE model assumes that tumor and immune cell populations are well-mixed. This does not hold for CAR T-cell treatment of solid tumors. However, starting with a non-spatial model allows us to mine relevant parameters from the literature, is simple enough to allow analysis, and can still provide useful insight.

Additionally, there are elements of cancer biology that are excluded from the model. Studies of CAR T-cell treatment have shown that a patient's homeostatic cytokine

profile is a key determinant of successful chemotherapeutic preconditioning for CAR T-cell therapy (Hirayama et al. 2019; Neelapu 2019; Rosenberg et al. 2008). Our model does not explicitly account for cytokines and other supporting immune molecules, but their influence shows up indirectly through competition between endogenous effector cells and CAR T-cells. A more detailed treatment of supporting immune molecules would be interesting, but for the sake of simplicity we exclude them here.

For our model, we also assume that all tumor cells are vulnerable to attack by the injected CAR T-cells. This may not necessarily be the case, for example, in the presence of resistance to CAR T-cell therapy. The model could be extended to include a subpopulation of cancer cells that are not recognized by the CAR T-cells, perhaps because they do not display the target ligand. This would be an interesting and relevant problem to address. Different types of CAR T-cells could also be compared by modifying the parameters describing CAR T-cell activity if there is appropriate data from cytotoxicity assays available.

CAR T-cells have transformed treatment of hematological cancers and show enormous potential for further innovation and application. One challenge facing this technology is the ubiquity of severe side-effects. Standard treatment protocol includes a chemotherapeutic preconditioning regimen, yet the optimal combination of chemotherapy and CAR T-cells to minimize side-effects, while maintaining efficacy has not been determined. Addressing the question of how these two forms of treatment interact for any given patient with a simple mathematical model takes an inexpensive first step towards informing further investigations.

Acknowledgements The authors would like to thank Kelsey Marcinko and Benjamin Liu for their helpful feedback during the writing process.

Code Availability For access to simulation code, please contact the authors.

Compliance with Ethical Standards

Conflict of interest The authors declare that they have no conflict of interest.

Appendix A: Model Analysis

Here, we present a linear stability analysis for our model post-treatment. Because the treatment plans we consider are generally confined to within 5–20 days total for both chemotherapy and CAR T-cell injection, the dose schedules, $\nu_M(t)$ and $\nu_C(t)$, are zero for t greater than 5–20 days. Furthermore, the chemotherapy plans used for lymphodepletion are on the shorter end of this, spanning only 3–5 days. When $\nu_M(t) = 0$, the concentration of chemotherapy rapidly declines to zero and the only possible chemotherapy concentration at equilibrium is $M(t) = 0$. Thus, we can characterize the relevant equilibria for our model scenarios by analyzing Sys. (2a-c) with $\nu_M(t) = 0$ and $\nu_C(t) = 0$,

$$\frac{\mathrm{d}T}{\mathrm{d}t} = aT(1-T) - D_E - D_C, \tag{6a}$$

$$\frac{\mathrm{d}E}{\mathrm{d}t} = g - j_E \frac{D_E^2}{k + D_E^2} \ln\left(\frac{E + C}{K}\right) E - q_E E T - m_E E, \tag{6b}$$

$$\frac{\mathrm{d}C}{\mathrm{d}t} = -j_C \frac{D_C^2}{k + D_C^2} \ln\left(\frac{E + C}{K}\right) C - q_C C T - m_C C, \tag{6c}$$

where D_E and D_C are still the tumor cell lysis terms,

$$D_E = d_E \frac{(E/T)^l}{s + (E/T)^l} T \quad \text{and} \quad D_C = d_C \frac{(C/T)^l}{s + (C/T)^l} T. \tag{7}$$

To begin our analysis, we first nondimensionalize Sys. (6) as follows. Let $x = bT$, $y = aE/g$, $z = aC/g$, $D_y = D_E/a$, $D_z = D_C/a$ and $t^* = at$. This results in twelve nondimensional parameters,

$$d_y = d_E/a, \quad d_z = d_C/a, \quad j_y = j_E/a, \quad j_z = j_C/a, \quad k^* = b^2 k/a^2,$$
$$K^* = aK/g,\ m_y = m_E/a,\ m_z = m_C/a,\ q_y = q_E/(ab),\ q_z = q_C/(ab),$$

and $s^* = s(a/(gb))^l$. The parameter l is nondimensional in the original system, and so remains unchanged. Dropping stars for notational simplicity, the nondimensionalized system without chemotherapy or additional CAR T-cell doses is given by

$$\frac{\mathrm{d}x}{\mathrm{d}t} = x(1 - x) - D_y - D_z, \tag{8a}$$

$$\frac{\mathrm{d}y}{\mathrm{d}t} = 1 - y\left(j_y \frac{D_y^2}{k + D_y^2} \ln\left(\frac{y + z}{K}\right) + q_y x + m_y\right), \tag{8b}$$

$$\frac{\mathrm{d}z}{\mathrm{d}t} = -z\left(j_z \frac{D_z^2}{k + D_z^2} \ln\left(\frac{y + z}{K}\right) + q_z x + m_z\right), \tag{8c}$$

where D_x and D_y are now dimensionless ratio terms,

$$D_y = d_y \frac{(y/x)^l}{s + (y/x)^l} x \quad \text{and} \quad D_z = d_z \frac{(z/x)^l}{s + (z/x)^l} x. \tag{9}$$

Next, we find the equilibria of the system, which occur at the intersections of the tumor, effector, and CAR T-cell nullclines, where $\dot{x} = 0$, $\dot{y} = 0$, and $\dot{z} = 0$, respectively. From Eq. (8a), we see that the tumor cell nullclines are $x = 0$ and

$$x = 1 - d_y \frac{(y/x)^l}{s + (y/x)^l} - d_z \frac{(z/x)^l}{s + (z/x)^l}. \tag{10}$$

For the effector cell nullcline, we set the right-hand side of Eq. (6b) equal to zero and find that $\dot{y} = 0$ when

$$y = \left(m_y + q_y x + j_y \frac{D_y^2}{k + D_y^2} \ln\left(\frac{y+z}{K} \right) \right)^{-1}. \tag{11}$$

From Eq. (8c), we can see that CAR T-cell population change will be zero when $z = 0$, or when the following implicit equation is satisfied

$$0 = m_z + q_z x + j_z \frac{D_z^2}{k + D_z^2} \ln\left(\frac{y+z}{K} \right). \tag{12}$$

We will refer to the intersection between the tumor nullcline $x = 0$, the effector cell nullcline, Eq. (11), and the CAR T-cell nullcline $z = 0$ as the zero-tumor or tumor-free equilibrium. We refer to equilibria that occur at the intersection between the tumor nullcline Eq. (10), the effector cell nullcline, Eq. (11), and the CAR T-cell nullcline $z = 0$ as nonzero-tumor boundary equilibria. Equilibria that occur at the intersection between the tumor nullcline Eq. (10), the effector cell nullcline, Eq. (11), and CAR T-cell nullcline Eq. (12) will be referred to as interior equilibria.

In order to determine the stability of the steady states, we apply linear stability analysis. The linearized system at point (x, y, z) is summarized by the Jacobian, H, of Sys. (8) evaluated at (x, y, z). Let

$$J_y = -j_y \frac{D_y^2}{k + D_y^2} \ln\left(\frac{y+z}{K} \right) y \quad \text{and} \quad J_z = -j_z \frac{D_z^2}{k + D_z^2} \ln\left(\frac{y+z}{K} \right) z \tag{13}$$

Then, the Jacobian of Eq. (8) evaluated at that point (x, y, z) is,

$$H|_{(x,y,z)} = \begin{pmatrix} 1 - \left(2x + \frac{\partial D_y}{\partial x} + \frac{\partial D_z}{\partial x} \right) & -\frac{\partial D_y}{\partial y} & -\frac{\partial D_z}{\partial z} \\ \frac{\partial J_y}{\partial x} - q_y y & \frac{\partial J_y}{\partial y} - q_y x - m_y & \frac{\partial J_y}{\partial z} \\ \frac{\partial J_z}{\partial x} - q_z z & \frac{\partial J_z}{\partial y} & \frac{\partial J_z}{\partial z} - q_z x - m_z \end{pmatrix}. \tag{14}$$

Let

$$H|_{(x,y,z)} = \begin{pmatrix} h_{11} & h_{12} & h_{13} \\ h_{21} & h_{22} & h_{23} \\ h_{31} & h_{32} & h_{33} \end{pmatrix},$$

so that substituting the partial derivatives into Eq. (14) gives

$$h_{11} = 1 - \left(2x + \frac{D_y}{x} \left(1 - \frac{ls}{s + (y/x)^l} \right) + \frac{D_z}{x} \left(1 - \frac{ls}{s + (z/x)^l} \right) \right), \tag{15a}$$

$$h_{12} = -D_y \left(\frac{ls}{s + (y/x)^l} \right), \tag{15b}$$

$$h_{13} = -D_z\left(\frac{ls}{s+(z/x)^l}\right) \tag{15c}$$

$$h_{21} = \frac{1}{x}\left(\frac{2kJ_y}{k+D_y^2}\left(\frac{ls}{s+(y/x)^l}-1\right)-q_y xy\right), \tag{15d}$$

$$h_{22} = \frac{J_y}{y}\left(1+\frac{2k}{k+D_y^2}\frac{ls}{s+(y/x)^l}\right)-m_y-q_y x-\frac{y}{K(y+z)}\frac{j_y D_y^2}{k+D_y^2} \tag{15e}$$

$$h_{23} = \frac{-j_y y}{y+z}\frac{D_y^2}{k+D_y^2} \tag{15f}$$

$$h_{31} = \frac{1}{x}\left(\frac{2kJ_z}{k+D_z^2}\left(\frac{ls}{s+(z/x)^l}-1\right)-q_z xz\right) \tag{15g}$$

$$h_{32} = \frac{-j_z z}{y+z}\frac{D_z^2}{k+D_z^2} \tag{15h}$$

$$h_{33} = \frac{J_z}{z}\left(1+\frac{2k}{k+D_z^2}\frac{ls}{s+(z/x)^l}\right)-m_z-q_z x-\frac{z}{K(y+z)}\frac{j_z D_z^2}{k+D_z^2} \tag{15i}$$

The simplest steady state to characterize is the tumor-free equilibrium. Evaluating the effector cell nullcline at $x = 0$ and $z = 0$ yields $y = 1/m_y$. Hence, the tumor-free equilibrium occurs at $(x_0^*, y_0^*, z_0^*) = (0, 1/m_y, 0)$. Linearizing about this point, the Jacobian is

$$H|_{\left(0,\frac{1}{m_y},0\right)} = \begin{pmatrix} 1-d_y-d_z & 0 & 0 \\ \frac{-q}{m_y} & -m_y & 0 \\ 0 & 0 & -m_z \end{pmatrix}, \tag{16}$$

which has eigenvalues $\lambda_1 = 1-d_z-d_y$, $\lambda_2 = -m_y$, and $\lambda_3 = -m_z$. The parameter values d_y, d_z, m_y, and m_z will always be positive real numbers. It follows that λ_1, λ_2 and λ_3 are always real and negative when $d_y + d_z > 1$. For the biologically relevant cases, we considered, the parameters $d_y > 1$ and $d_z > 1$, so this condition is satisfied. Hence, the equilibrium point will be a stable node, which aligns with the results reported by de Pillis et al. for their 2006 model. The stability of the tumor-free equilibrium reflects the idea that, once activated, the immune system can contain a tumor if it is small enough.

Now we turn our attention to the nonzero-tumor boundary equilibria. For these equilibria, $z = 0$ still, but now

$$x = 1-D_y-D_z = 1-d_y\frac{(y/x)^l}{s+(y/x)^l}. \tag{17}$$

In this case, we can solve Eq. 17 for y as a function of x along the tumor nullcline,

$$L_1(x) = \left(\frac{s(1-x)x^l}{d_y-(1-x)}\right)^{1/l}. \tag{18}$$

Substituting Eq.(17) and $z = 0$ into the effector cell nullcline yields an implicit curve in the plane $z = 0$,

$$L_2(x, y): \quad y = \left(m_y + q_y x + j_y \frac{(1-x)^2 x^2}{k + (1-x)^2 x^2} \ln\left(\frac{y}{K}\right) \right)^{-1}. \tag{19}$$

The nonzero tumor boundary equilibrium points are the intersections of Eqs. (18) and (19) for each set of parameters. See Fig. 1a for a plot of $L_1(x)$ (tumor cell nullcline) and $L_2(x, y)$ (effector cell nullcline) for the Patient 3 parameters with equilibria marked. For reasonable parameter ranges, reported in Table 1, we observed that the model has two positive nonzero tumor equilibrium points in the plane $z = 0$ because the parameter s is large enough that $L_1(x)$ exceeds $L_2(x, y)$ for most of the interval $x \in (0, 1)$, but $L_1(0) = 0 < L_2(0, 1/m)$ and $L_1(1) = 0 < L_2(1, y^*)$.

The first nonzero tumor boundary equilibrium occurs at a large number of tumor cells, $x_1^* \approx 1$, a small number of effector cells, $y_1^* \approx L_1(1) = 1/(q + m)$, and $z_1^* = 0$. Due to the location near the tumor cell carrying capacity, we call this the high-tumor equilibrium. The second nonzero tumor boundary equilibrium occurs at a small number of tumor cells, a moderate number of effector cells and $z = 0$. Although it is not possible to find exact, closed-form expressions for the nonzero tumor boundary equilibria because it requires finding the roots of a quintic polynomial, we can use the Routh–Hurwitz criterion to find conditions under which the high-tumor equilibrium is stable (Wiggins 2003, p. 14). Let $\tau(M)$ denote the trace of a matrix M and $\Delta(M)$ denote the determinant of a matrix M. For a three-dimensional system, the Routh–Hurwitz criterion says that all eigenvalues of matrix H will have negative real part if the following criteria are satisfied,

1. $\tau(H) < 0$,
2. $\Delta(H) < 0$,
3. $\tau(H^2) - \tau(H)^2 < 2\Delta(H)/\tau(H)$.

First, we use the nullclines to simplify the Jacobian. Substituting $z = 0$ and $D_y = (1 - x)x$ from Eq. (17) into Sys. (16), the Jacobian has entries

$$h_{11} = -x + \frac{ls(1-x)}{s + (y/x)^l}, \tag{20a}$$

$$h_{12} = -x\left(\frac{ls(1-x)}{s + (y/x)^l}\right), \tag{20b}$$

$$h_{13} = 0 \tag{20c}$$

$$h_{21} = \frac{1}{x}\left(\frac{2kJ_y}{k + (1-x)^2x^2}\left(\frac{ls}{s + (y/x)^l} - 1\right) - q_y xy\right), \tag{20d}$$

$$h_{22} = \frac{J_y}{y}\left[\left(\frac{2k}{k + (1-x)^2x^2}\right)\left(\frac{ls}{s + (y/x)^l}\right) + 1\right] - q_y x - m_y - \frac{j_y}{K}\left(\frac{(1-x)^2x^2}{k + (1-x)^2x^2}\right) \tag{20e}$$

$$h_{23} = -j_y \frac{(1-x)^2 x^2}{k + (1-x)^2 x^2} \tag{20f}$$

$$h_{31} = 0 \tag{20g}$$

$$h_{32} = 0 \tag{20h}$$

$$h_{33} = -m_z - q_z x \tag{20i}$$

Before applying the Routh–Hurwitz criterion, we will need to compute $\tau(H)$, $\Delta(H)$, and $\tau(H^2)$. The trace of the Jacobian is

$$\tau(H) = h_{11} + h_{22} + h_{33}. \tag{21}$$

This will be negative, satisfying criterion 1, when the three diagonal entries are negative. Next, consider the determinant of the Jacobian

$$\Delta(H) = h_{11}h_{22}h_{33} - h_{12}h_{21}h_{33}, \tag{22}$$

due to zero entries in the Jacobian. Furthermore, with $x \approx 1$, h_{12} will be very nearly 0 and so we can consider

$$\Delta(H) = h_{11}h_{22}h_{33}. \tag{23}$$

Hence, the determinant will also be negative, satisfying criterion 2, when the three diagonal entries share the same sign. Squaring H and summing the diagonal entries yields

$$\tau(H^2) = h_{11}^2 + h_{22}^2 + h_{33}^2 + 2h_{12}h_{21} \tag{24}$$

$$= h_{11}^2 + h_{22}^2 + h_{33}^2, \tag{25}$$

again because h_{12} goes to zero for $x \approx 1$. We know that $\Delta(H)/\tau(H) > 0$ when both are negative, so showing $\tau(H^2) < \tau(H)^2$ will be sufficient to satisfy the third criterion if the first two are met. Squaring $\tau(H)$ yields

$$\tau(H)^2 = h_{11}^2 + h_{22}^2 + h_{33}^2 + 2h_{11}h_{22} + 2h_{22}h_{33} + 2h_{11}h_{33}. \tag{26}$$

All the terms in the sum will be positive when $h_{11} < 0$, $h_{22} < 0$, and $h_{33} < 0$ in which case it is clear that $\tau(H^2) < \tau(H)^2$. Thus, all three of the Routh–Hurwitz criterion will hold when the three diagonal entries of H are negative.

We start with the first diagonal entry. From Eq. (20a), we can see that when $x \approx 1$ it follows that that $h_{11} \approx -1$.

Next, we consider the second diagonal entry, h_{22}, defined in Eq. (20e). Substituting in $J_y/y = 1/y - m_y - q_y x$ yields,

$$\begin{aligned} h_{22} = \frac{1}{y}\left[\left(\frac{2k}{k+(1-x)^2x^2}\right)\left(\frac{ls}{s+(y/x)^l}\right)+1\right] \\ -(q_y x + m_y)\left[\left(\frac{2k}{k+(1-x)^2x^2}\right)\left(\frac{ls}{s+(y/x)^l}\right)+2\right] \\ -\frac{j_y}{K}\left(\frac{(1-x)^2x^2}{k+(1-x)^2x^2}\right) \end{aligned} \tag{27}$$

Then, noting that the final term will be negative, but close to zero and that the first fractional term will approach 2 when $x \approx 1$, h_{22} will be less than 0 when

$$\frac{1}{y} < (q_y + m_y)\frac{2\left(\frac{ls}{s+(y/x)^l}\right)+2}{2\left(\frac{ls}{s+(y/x)^l}\right)+1}. \tag{28}$$

Hence, when $x \approx 1$, the entry h_{22} will be negative when

$$y > \frac{1}{q_y + m_y}. \tag{29}$$

Finally, from Eq. (20i), we can see that for any positive value of x, including $x \approx 1$, $h_{33} < 0$ because both parameter values, m_z and q_z, are real and positive.

Thus, when $z = 0$, $x \approx 1$, and $y > 1/(q_y + m_y)$, the diagonal entries of H, h_{11}, h_{22} and h_{33}, will all be negative. Hence, the Routh–Hurwitz Criterion will be satisfied and all eigenvalues of the system will have negative real parts. These conditions are satisfied by the high-tumor equilibrium for the patient parameters considered here, so it follows by the Routh–Hurwitz criterion that the high-tumor steady state is stable.

Characterizing the interior equilibria analytically is intractable. However, we located equilibria at the intersection of nullsurfaces, and characterized their stability numerically. For the parameter sets considered here, there are up to four interior equilibria with $x \geq 0$, $y \geq 0$, and $z \geq 0$. To explore these equilibria, we constructed a bifurcation diagram by varying the maximum CAR T-cell recruitment rate, j_C, from 0 to 3 while holding all other parameters at their Patient 3 value (Fig. 1c). With strictly positive parameter values, an unstable node and a saddle point are present at a low (but nonzero) population level for all three cell types. The stable manifold of this saddle point separates the basin of attraction for healthy outcomes from the basin of attraction for unhealthy outcomes. Increasing j_C causes this saddle point to move towards larger tumor and CAR T-cell values as the nonzero CAR T-cell nullcline shifts upward with respect to tumor and CAR T-cells. For the patient 3 values, a saddle node bifurcation occurs when $j_C = 0.5105$ and a stable node appears simultaneously with another saddle point near the tumor cell carrying capacity. The stable manifold of this saddle point separates the basins of attraction for the high-tumor equilibrium from the basin of attraction for this new, stable coexistence equilibrium. Figure 1b shows the null

surfaces with the unperturbed patient 3 parameter set, i.e., with $j_C = 0.6$, so all four interior equilibria are visible. Continuing to increase j_C past the point $j_C = 2.56$, the nonzero CAR T-cell nullcline shifts far enough upward with respect to tumor and CAR T-cells that the stable coexistence equilibrium and the saddle node at high CAR T-cell values collide and disappear in another saddle-node bifurcation. This leaves two remaining unstable interior equilibria, and the stable manifold of the remaining saddle node now separates the basins of attraction for the low tumor and high-tumor equilibria. Varying other parameters associated with CAR T-cells can also shift the nonzero CAR T-cell nullsurface through this sequence of bifurcations.

The positive quadrant is an invariant set of system 6. In order for a trajectory to leave the first quadrant, it would have to cross an axis, which requires $\dot{x} < 0$ somewhere along the $x = 0$ axis, $\dot{y} < 0$ somewhere along the $y = 0$ axis or $\dot{z} < 0$ somewhere along the $z = 0$ axis. However, when $x = 0$ it is clear from Eq. (6a) that $\dot{x} = 0$. From Eq. (6b), we can also see that when $y = 0$, it follows that $\dot{y} = 1$, which is positive. And when $z = 0$, $\dot{z} = 0$ also.

Appendix B: Parameter Selection

We selected parameters based on previous models in the literature. The metastatic melanoma parameter sets came directly from the parameter values for Patients 9 and 10 in the governing equations for tumor cells and $CD8^+$ T-cells reported by de Pillis et al. (2005). However to counteract the effect of eliminating the other immune cell types (NK cells and circulating lymphocytes) that stimulate $CD8^+$T cells, the base recruitment rate of effector cells from Kuznetsov et al. (1994) was taken to be the base recruitment rate of effector cells for Patients 3 and 4.

We set the parameter values for our diffuse large B-cell lymphoma patient, Patient 1, to the midpoint of the ranges reported by Rösch et al. (2016) when there was an analogous term. We could use most parameters directly from Rösch et al. (2016). However, the parameters involved in the novel tumor-cell lysis term introduced by de Pillis et al. did not correspond directly to parameters in Rösch's model. We expect endogenous T-cells in lymphoma patients to be less effective at killing tumor cells than CAR T-cells, so we set $d_E = 2.02$, or roughly 90% as effective as CAR T-cells. We set the remaining two parameters, l and s, to the average of the two patients considered in the model from de Pillis et al. (2005). The Rösch et al. model assumed exponential tumor growth, rather than logistic so we set $b = 5 \times 10^{-13}$ because this choice allows tumor cells to exhibit essentially exponential growth towards the number of lymphocytes in the body in the absence of an immune response.

The chronic lymphocytic leukemia patient parameter values were set to the midpoint of the ranges reported by Nanda et al. (2013) when there was an analogous term, adjusting for differences in units. The Nanda et al. model also assumed exponential tumor growth, rather than logistic so we set $b = 5 \times 10^{-13}$. Under the same reasoning as the lymphoma parameters, we set $d_E = 2.02$, and set the final parameters involved in the novel interaction term (l and s) to the average of the two patients considered in the model from de Pillis et al. (2005).

CAR T-cell parameters that differ from their corresponding parameter in the endogenous effector cells (d_C, m_C, j_C, and q_C) were determined from the values reported by Kimmel et al. (2019). For all patients, the CAR T-cell death rate and the maximum CAR T-cell kill rate were set to the median value for their deterministic model, converting units if necessary. Note that the maximum tumor kill rate is lower for CAR T-cells than for endogenous effector cells in the metastatic melanoma patients. This may seem counter-intuitive; however, the parameter values from de Pillis et al. (2005) were fit to clinical trials of successful tumor infiltrating lymphocyte (TIL) treatment. TILs are currently more effective than CAR T-cells against metastatic melanoma (Itzhaki et al. 2020). The CAR T-cell exhaustion rate and the effector cell carrying capacity for blood cancers (Patients 1 and 2), came from converting the corresponding values in the model from Kimmel et. al (2019) to the our units. For the metastatic melanoma parameter sets (Patient 3 and 4), we use a higher inactivation rate so that the order of magnitude of the ratio of the tumor carrying capacity to deactivation is preserved. Numerous studies have shown the microenvironment around solid tumors to be more hostile to immune cells than in the case of hematologic cancers (Villanueva and Herlyn 2008). For metastatic melanoma patients we also was scaled down the carrying capacity of effector cells by 10% to account for the lower access of T-cells to solid tumor cells (Villanueva and Herlyn 2008; Jorge et al. 2020). In their model, Kimmel et al. (2019) use a functional form which places our maximum CAR T-cell recruitment rate, j_C, in the interval [0.11, 1.31]. We chose to set the CAR T-cell recruitment rate to be a factor larger than the endogenous cell recruitment rate: $j_C = 22 j_E$. The choice of 22 as a scale factor places the resulting values within the range reported by Kimmel et al. and produces simulation results spanning an interesting range of biological outcomes.

The kill parameters relating to chemotherapy were taken from de Pillis et al. (2006), since the patients in the metastatic melanoma study were also treated with fludarabine. The fractional cell kills used by de Pillis et al. were $K_T = 0.9$ and $K_E = 0.6$ which assumes that chemotherapy is one log-kill and that it kills a larger fraction of tumor cells than host cells. However, to reflect the fact that CAR T-cell treatment is commonly used for patients whose disease is less responsive to chemotherapy, we reduced K_T to 0.7. We set $K_C = K_E = 0.6$, therein assuming that CAR T-cells will be impacted by chemotherapy at the same rate as endogenous T-cells. The decay rate γ can be calculated from the half-life of a substance, τ, by $\gamma = \ln(2)/\tau$. The choice of strength for chemotherapy regimens was chosen by working backwards to see what values resulted in reasonable concentrations of fludarabine building up in the system, where "reasonable" concentrations matched those reported by Ju et al. in a pharmacokinetic study of the drug (2014). For 25 mg of fludarabine administered over one half hour each day for 5 days, Ju et al. reported a peak concentration of $C_{\max} = 1222(668 - 1732)\text{ng/mL} = 3.34\ \mu\text{M}$. We found that a dose strength of $S = 77\ \mu\text{Mday}^{-1}$ achieved this $C_{\max}$ in our simulations, so this was used as medium strength. The high strength was set to be $S = 125\ \mu\text{Mday}^{-1}$ in order to achieve the same area under the concentration curve with only 3 days of injections. If we chose to instead match the dose administered (area under $\nu_M(t)$) between the two plans, the patient outcomes were qualitatively similar.

Note that while the treatment parameters are well-founded in pharmacokinetic data, the patient parameters have been drawn from previous theoretical studies for different

cancer types. Some have been fit to patient data, but not all. In order to strengthen the impact of any suggestions made by this model, it remains to calibrate parameters model to data from previous CAR T cell therapy patients and validate the model by evaluating its predictive performance on untrained data.

Appendix C: Numerical Simulations and Sensitivity Analysis

We implemented numerical simulations with parameters for Patient 1–4 listed in Table 1 using a combination of fourth order Runge–Kutta integration schemes in MATLAB. During chemotherapy, we enforced a fixed step size of $\mathrm{d}t = 0.0208$ corresponding to approximately one half hour or $1/48$ of a day using ode4(). The remainder of each simulation was completed with ode45(), which dynamically chooses the time-step.

To discover which components of the model contribute most significantly to the effectiveness of CAR T-cell injections, we performed a numerical sensitivity analysis assessing how the model parameters impact the shape of the separatrix between the basin of attraction for the high-tumor equilibrium and the basin of attraction for the tumor-free equilibrium.

As a baseline for Patients 1–4, we calculated the precise threshold of CAR T-cells above which a patient initial condition will move towards the healthy, tumor-free equilibrium when the system starts at the low-TB initial condition. We call this number of effector cells the CAR T-cell success threshold, because any treatment plan which injects a dose of CAR T-cells exceeding this quantity will be successful (in theory) against tumor burdens up to and including the low TB, (Fig. 7a). For the reasonable patient initial conditions considered in our simulations, post-chemotherapy tumor burdens generally fell below the low TB value at the time of CAR T-cell injection. After calculating the threshold with unperturbed parameters, each parameter was increased by 1% while holding all other parameter values constant. The relative change in the CAR T-cell success threshold was computed by subtracting the unperturbed CAR T-cell success threshold from the perturbed CAR T-cell success threshold and dividing the difference by the unperturbed threshold. The same procedure was followed for a 1% decrease in each parameter. The results of sensitivity analysis for Patient 1 are shown in Fig. 7b and the results for Patients 2–4 are shown in Fig. 8.

For all patients, varying the tumor growth rate, a, had a significant impact on the CAR T-cell success threshold, indicating that cancers characterized by a higher growth rate will require higher CAR T-cell doses if administered at the same patient initial condition. In contrast with Patients 1–2, the tumor carrying capacity, $1/b$, also had a non-negligible effect on the success threshold for Patients 3–4. This seems to be a consequence of the fact that the low TB condition is only one order of magnitude below the tumor carrying capacity for Patient's 3 and 4, so the behavior of the tumor population can enter the saturating regime of logistic growth, shaped by the carrying capacity.

The parameters characterizing the activity of CAR T-cells also have a nonnegligible impact on the success threshold. For all patients, changing the exponent in the tumor cell lysis rate, l, has the largest impact on the CAR T success threshold, with a 1%

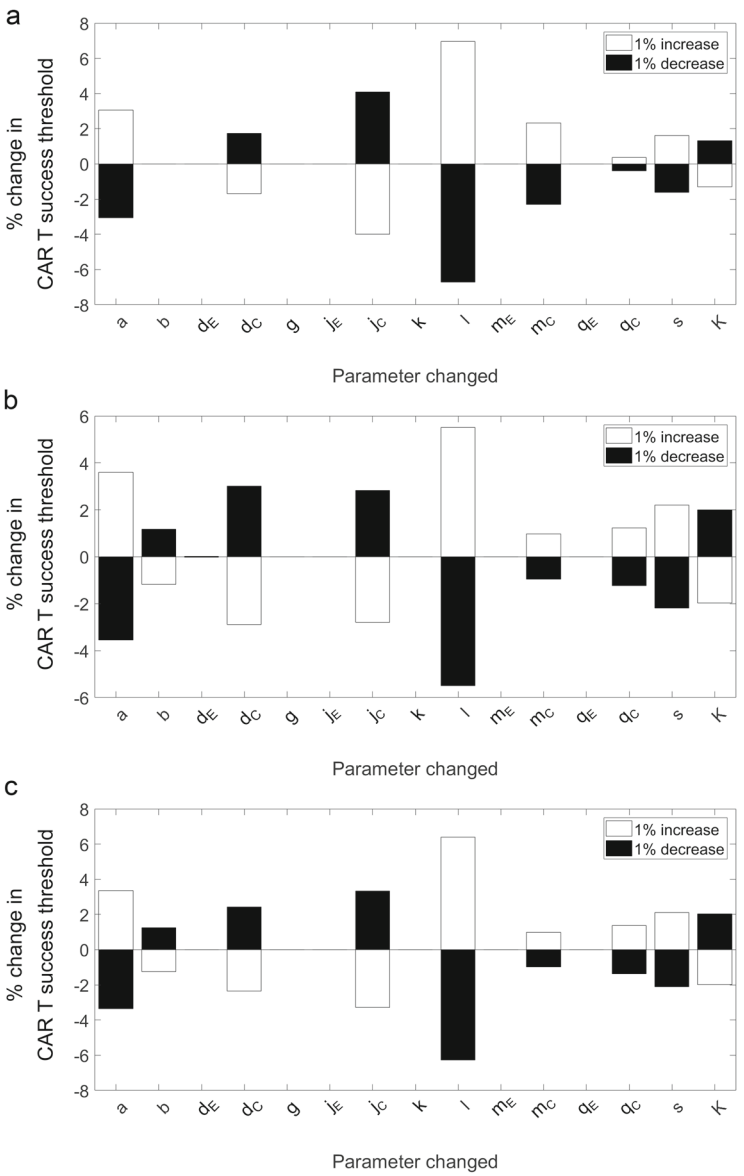

Fig. 8 Results of sensitivity analysis for **a** Patient 2, **b** Patient 3, and **c** Patient 4. The dose of CAR T-cells required to achieve a healthy patient outcome from the low tumor initial condition is most sensitive to the tumor growth rate, a, and the exponent of the tumor cell lysis rate, l (a parameter associated with the cooperativity of CAR T-cells). Other parameters dictating the behavior of CAR T-cells also have a non-negligible impact on the CAR T-cell success threshold. The inverse of the tumor cell carrying capacity, b, has little effect on the threshold for Patients 1–2, but a noticeable effect for Patients 3–4. It is worth noting that the low tumor initial condition is relatively close to the tumors carrying capacity for Patients 3–4 compared to Patients 1–2

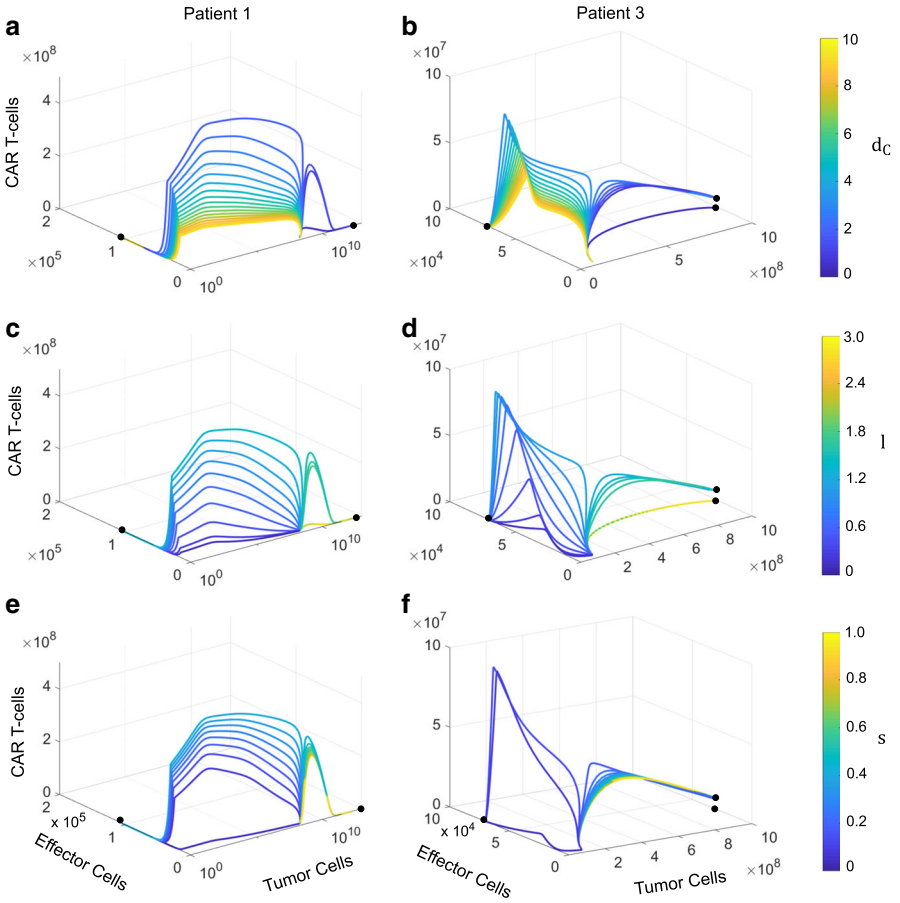

Fig. 9 Impact of varying parameters characterizing the lysis of tumor cells by CAR T-cells on patient trajectories initiated at ($T_0 = 5 \times 10^8$, $E_0 = 3 \times 10^4$, $C_0 = 10^6$) for Patient 1 and ($T_0 = 10^8$, $E_0 = 3 \times 10^4$, $C_0 = 10^6$) for Patient 3. The maximum tumor cell lysis rate, d_C, was varied between 0 and 10 for **a** Patient 1 and **b** Patient 3. At low values of d_C, trajectories approach an unhealthy patient outcome. As d_C increases, CAR T-cells are able to mount a larger response against the tumor, and eventually trajectories transition to approaching the healthy outcome. Continuing to increase d_C, CAR T-cells eradicate the tumor more quickly and with a smaller peak. The exponent in the tumor cell lysis rate, l, was varied from 0 to 3 for **c** Patient 1 and **d** Patient 3. For low values of l, CAR T-cells effectively kill tumor cells independently so trajectories rapidly reach the zero-tumor burden with low spikes in CAR T-cells. As l increases, higher cooperation between CAR T-cells is required and so larger peaks in CAR T-cells are seen. Eventually, the level of cooperation required is too high, and trajectories now approach an unhealthy outcome, though CAR T-cells still increase initially. Once $l > 2$, the CAR T-cells no longer spike after injection, as trajectories quickly approach the high-tumor state. The half-saturation value in the tumor cell lysis rate, s, was varied from 0 to 1 for **e** Patient 1 and **f** Patient 3. Increasing s increases the effector-target ratio required to reach the saturation regime of tumor cell lysis. For low values of s the tumor is eradicated quickly with few CAR T-cells. As s increases, more CAR T-cells are required to eliminate the tumor observed in larger CAR T-cell peaks, until eventually this dose of CAR T-cells can no longer mount an effective response to this tumor burden. Further increasing s decreases the peak of the failed response

change in l leading to a 5–7% change in the threshold. The parameter l encodes how the lysis rate depends on the ratio of CAR T-cells/tumor cells. Thinking of this ratio as a chemical concentration we can think of varying l as allowing the expression D to range between non-cooperative (completely independent) binding between CAR T-cells and surface antigens on the tumor cells when $l = 1$, and cooperative binding when $l > 1$. The fact that a 1% change in l can result in a 7% shift in the threshold indicates that small changes in CAR T-cell cooperativity will affect clinical outcomes. For Patients 1–2, and 4, the next most inlfuential parameter is the maximum recruitment rate of CAR T-cells, j_C. Larger values of j_C decrease the necessary injected dose of CAR T-cells because those cells that are injected are able to expand further. For Patient 3, perturbations to the maximum tumor kill rate by CAR T-cells, d_C, have the most outsized impact after l. This parameter defines the upper limit of the ratio-dependent cell-lysis term, suggesting that small improvements to the effectiveness of CAR T-cell activity could significantly reduce the dose required by patients.

Sensitivity analysis based on the high tumor burden indicated that the parameters associated with tumor cell lysis by CAR T-cells, d_C, l, and s, play an important role in the success of CAR T-cell treatment so we performed further numerical investigations to show how varying these parameters impacts patient trajectories. Figure 9 shows patient trajectories resulting from running simulations with the Patient 1 and Patient 3 parameter sets from an initial condition near the separatrix between the basins of attraction for the different equilibria. Either d_C, l, or s was varied through a relevant range while holding all other parameter values constant at the value listed in Table 1 and the trajectories were color coded according to the value of the parameter in question.

First the maximum tumor cell lysis rate, d_C, was varied between 0 and 10. When tumor cell lysis is zero, the CAR T-cell recruitment is also affected, and CAR T-cells cannot proliferate so the trajectory proceeds in the $C = 0$ plane to the high-tumor equilibrium. As d_C increases a larger spike in CAR T-cells is seen. Though trajectories still reach the high-tumor equilibrium for Patient 1, they now approach the unhealthy coexistence equilibrium for Patient 3. Eventually the maximum kill rate is high enough that a large spike in CAR T-cells is sufficient to move the patient to the healthy zero-tumor outcome. Continuing to increase d_C the system approaches the healthy zero-tumor equilibrium faster and with a shorter and shorter spike in CAR T-cells.

Next, the exponent in the tumor cell lysis rate, l, was varied from 0 to 3. When $l = 0$, with even one CAR T-cell present tumor cells are killed at a rate independent of further increases in CAR T-cells. Consequently, the tumor is eradicated very quickly with very little expansion of CAR T-cells beyond the initial dose. As l increases more cooperation is required between CAR T-cells to attack tumor cells, so we see larger and larger spikes in CAR T-cells needed to contain the tumor and reach a healthy outcome. Eventually, the level of cooperativity required is too great for this CAR T-cell dose to handle this tumor burden. At this point, even though CAR T-cells expand post injection, trajectories approach an unhealthy outcome. Once l is greater than 2, the injection of CAR T-cells has virtually no effect on the disease, and CAR T-cells and tumor cells monotonically approach the high-tumor equilibrium.

The half-saturation value in the tumor cell lysis rate, s, was varied from 0 to 1. Increasing s increases the effector target ratio required to reach the saturation regime of tumor cell lysis. When $s = 0$, the lysis of tumor cells by CAR T-cells transitions to

the saturation regime immediately and so the tumor is eradicated rapidly by a small number of CAR T-cells. As s increases, the CAR T-cell to tumor cell ratio needed to reach the saturation kill rate increases, and the eradication time and fold-increase in CAR T-cells increases along with it. At a critical value around $s = 0.5$ for Patient 1 and $s = 0.25$ for Patient 3, trajectories now approach an unhealthy outcome and the peak CAR T-cell population decreases as s increases. The effector to target ratio required to reach the saturation regime is now too high for this dose to handle this initial condition.

References

Almåsbak H, Aarvak T, Vemuri MC (2016) CAR T cell therapy: a game changer in cancer treatment. J Immunol Res

Borges FS, Iarosz K, Ren HP, Batista AM, Baptista MS, Viana RL, Lopes S, Grebogi C (2014) Model for tumour growth with treatment by continuous and pulsed chemotherapy. Biosystems 116:43–48

Brady R, Enderling H (2019) Mathematical models of cancer: When to predict novel therapies, and when not to. Bull Math Biol 81(10):3722–3731

Brown CE, Mackall CL (2019) CAR T cell therapy: inroads to response and resistance. Nat Rev Immunol 19(2):73

Eftimie R, Bramson JL, Earn DJ (2011) Interactions between the immune system and cancer: a brief review of non-spatial mathematical models. Bull Math Biol 73(1):2–32

Gardner SN (2000) A mechanistic, predictive model of dose-response curves for cell cycle phase-specific and-nonspecific drugs. Cancer Res 60(5):1417–1425

Hardiansyah D, Ng CM (2019) Quantitative systems pharmacology model of chimeric antigen receptor T-cell therapy. Clin Transl Sci 12(4):343–349

Harlin H, Meng Y, Peterson AC, Zha Y, Tretiakova M, Slingluff C, McKee M, Gajewski TF (2009) Chemokine expression in melanoma metastases associated with CD8+ T-cell recruitment. Cancer Res 69(7):3077–3085

Harris DT, Hager MV, Smith SN, Cai Q, Stone JD, Kruger P, Lever M, Dushek O, Schmitt TM, Greenberg PD et al (2018) Comparison of T cell activities mediated by human TCRs and CARs that use the same recognition domains. J Immunol 200(3):1088–1100

Hirayama AV, Gauthier J, Hay KA, Voutsinas JM, Wu Q, Gooley T, Li D, Cherian S, Chen X, Pender BS et al (2019) The response to lymphodepletion impacts PFS in patients with aggressive non-Hodgkin lymphoma treated with CD19 CAR t cells. Blood 133(17):1876–1887

Hopkins B, Tucker M, Pan Y, Fang N, Huang Z (2018) A model-based investigation of cytokine storm for T-cell therapy. IFAC-PapersOnline 51(19):76–79

Huang A, Golumbek P, Ahmadzadeh M, Jaffee E, Pardoll D, Levitsky H (1994) Role of bone marrow-derived cells in presenting MHC class I-restricted tumor antigens. Science 264(5161):961–965

Itzhaki O, Jacoby E, Nissani A, Levi M, Nagler A, Kubi A, Brezinger K, Brayer H, Zeltzer La, Rozenbaum M, et al. (2020) Head-to-head comparison of in-house produced CD19 CAR T-cell in ALL and NHL patients. J Immunother Cancer 8(1)

Jorge NA, Cruz JG, Pretti MAM, Bonamino MH, Possik PA, Boroni M (2020) Poor clinical outcome in metastatic melanoma is associated with a microRNA-modulated immunosuppressive tumor microenvironment. J Transl Med 18(1):1–17

Ju HY, Lee JW, Hong CR, Kim H, Park KD, Shin HY, Kim S, Jang K, Yu KS, Jang IJ, et al. (2014) Pharmacokinetics of fludarabine in pediatric hematopoietic stem cell transplantation

June CH, Sadelain M (2018) Chimeric antigen receptor therapy. New England J Med 379(1):64–73

Kalos M, Levine BL, Porter DL, Katz S, Grupp SA, Bagg A, June CH (2011) T cells with chimeric antigen receptors have potent antitumor effects and can establish memory in patients with advanced leukemia. Sci Transl Med 3(95):95ra73

Khalil DN, Smith EL, Brentjens RJ, Wolchok JD (2016) The future of cancer treatment: immunomodulation, CARs and combination immunotherapy. Nat Rev Clin Oncol 13(5):273

Kimmel GJ, Locke FL, Altrock PM (2019) Evolutionary dynamics of CAR T cell therapy. BioRxiv 717074

Kirschner D, Panetta JC (1998) Modeling immunotherapy of the tumor-immune interaction. J Math Biol 37(3):235–252
Kite (2017) Yescarta (axicabtagene ciloleucel) highlights of prescribing information. https://www.fda.gov/media/108377/download
Kochenderfer JN, Wilson WH, Janik JE, Dudley ME, Stetler-Stevenson M, Feldman SA, Maric I, Raffeld M, Nathan DAN, Lanier BJ et al (2010) Eradication of B-lineage cells and regression of lymphoma in a patient treated with autologous T cells genetically engineered to recognize CD19. Blood J Am Soc Hematol 116(20):4099–4102
Kochenderfer JN, Somerville RP, Lu T, Shi V, Bot A, Rossi J, Xue A, Goff SL, Yang JC, Sherry RM et al (2017) Lymphoma remissions caused by anti-CD19 chimeric antigen receptor T cells are associated with high serum interleukin-15 levels. J Clin Oncol 35(16):2017
Kruger S, Ilmer M, Kobold S, Cadilha BL, Endres S, Ormanns S, Schuebbe G, Renz BW, Dhaese JG, Schloesser H et al (2019) Advances in cancer immunotherapy 2019-latest trends. J Exp Clin Cancer Res 38(1):268
Kuznetsov VA, Makalkin IA, Taylor MA, Perelson AS (1994) Nonlinear dynamics of immunogenic tumors: parameter estimation and global bifurcation analysis. Bull Math Biol 56(2):295–321
Mahadeo KM, Khazal SJ, Abdel-Azim H, Fitzgerald JC, Taraseviciute A, Bollard CM, Tewari P, Duncan C, Traube C, McCall D et al (2019) Management guidelines for paediatric patients receiving chimeric antigen receptor T cell therapy. Nat Rev Clin Oncol 16(1):45–63
Miller KD, Nogueira L, Mariotto AB, Rowland JH, Yabroff KR, Alfano CM, Jemal A, Kramer JL, Siegel RL (2019) Cancer treatment and survivorship statistics. CA Cancer J Clin 69(5):363–385
Mokhtari RB, Homayouni TS, Baluch N, Morgatskaya E, Kumar S, Das B, Yeger H (2017) Combination therapy in combating cancer. Oncotarget 8(23):38022
Nanda S, de Pillis LG, Radunskaya AE (2013) B cell chronic lymphocytic leukemia-a model with immune response
Neelapu SS (2019) CAR T efficacy: Is conditioning the key? Blood J Am Soc Hematol 133(17):1799–1800
Novartis (2017) Kymriah (tisagenlecleucel) highlights of prescribing information. https://www.fda.gov/files/vaccines%2C%20blood%20%26%20biologics/published/Package-Insert---KYMRIAH.pdf
Palmer AC, Sorger PK (2017) Combination cancer therapy can confer benefit via patient-to-patient variability without drug additivity or synergy. Cell 171(7):1678–1691
Pandya PH, Murray ME, Pollok KE, Renbarger JL (2016) The immune system in cancer pathogenesis: potential therapeutic approaches. J Immunol Res
Pettitt D, Arshad Z, Smith J, Stanic T, Holländer G, Brindley D (2018) CAR T cells: a systematic review and mixed methods analysis of the clinical trial landscape. Mol Ther 26(2):342–353
de Pillis LG, Radunskaya AE, Wiseman CL (2005) A validated mathematical model of cell-mediated immune response to tumor growth. Cancer Res 65(17):7950–7958
de Pillis LG, Gu W, Radunskaya AE (2006) Mixed immunotherapy and chemotherapy of tumors: modeling, applications and biological interpretations. J Theor Biol 238(4):841–862
Pinho STRd, Freedman H, Nani F (2002) A chemotherapy model for the treatment of cancer with metastasis. Math Comput Model 36(7–8):773–803
Ribba B, Kaloshi G, Peyre M, Ricard D, Calvez V, Tod M, Čajavec-Bernard B, Idbaih A, Psimaras D, Dainese L et al (2012) A tumor growth inhibition model for low-grade glioma treated with chemotherapy or radiotherapy. Clin Cancer Res 18(18):5071–5080
Rodrigues BJ, Barros LRC, Almeida RC (2019) Three-compartment model of CAR T-cell immunotherapy. BioRxiv 779793
Rohrs JA, Wang P, Finley SD (2019) Understanding the dynamics of T-cell activation in health and disease through the lens of computational modeling. JCO Clin Cancer Inform 3:1–8
Rösch K, Scholz M, Hasenclever D (2016) Modeling combined chemo-and immunotherapy of high-grade non-hodgkin lymphoma. Leukemia & Lymphoma 57(7):1697–1708
Rosenberg SA, Restifo NP, Yang JC, Morgan RA, Dudley ME (2008) Adoptive cell transfer: a clinical path to effective cancer immunotherapy. Nat Rev Cancer 8(4):299–308
Sahoo P, Yang X, Abler D, Maestrini D, Adhikarla V, Frankhouser D, Cho H, Machuca V, Wang D, Barish M et al (2020) Mathematical deconvolution of CAR T-cell proliferation and exhaustion from real-time killing assay data. J R Soc Interface 17(162):20190734
Smith-Garvin JE, Koretzky GA, Jordan MS (2009) T cell activation. Ann Rev Immunol 27:591–619
Stein AM, Grupp SA, Levine JE, Laetsch TW, Pulsipher MA, Boyer MW, August KJ, Levine BL, June CH, Tomassian L et al (2017) CTL019 model-based cellular kinetic analysis of chimeric antigen receptor

(CAR) T cells to characterize the impact of tocilizumab on expansion and to identify correlates of cytokine release syndrome severity. Blood 130(Supplement 1):2561
Stein AM, Grupp SA, Levine JE, Laetsch TW, Pulsipher MA, Boyer MW, August KJ, Levine BL, Tomassian L, Shah S et al (2019) Tisagenlecleucel model-based cellular kinetic analysis of chimeric antigen receptor-T cells. CPT Pharm Syst Pharmacol 8(5):285–295
Talkington A, Dantoin C, Durrett R (2018) Ordinary differential equation models for adoptive immunotherapy. Bull Math Biol 80(5):1059–1083
Thommen DS, Schumacher TN (2018) T cell dysfunction in cancer. Cancer Cell 33(4):547–562
Turtle CJ, Hanafi LA, Berger C, Gooley TA, Cherian S, Hudecek M, Sommermeyer D, Melville K, Pender B, Budiarto TM et al (2016) CD19 CAR T cells of defined CD4+: CD8+ composition in adult b cell all patients. J Clin Investig 126(6):2123–2138
Usher J (1994) Some mathematical models for cancer chemotherapy. Comput Math Appl 28(9):73–80
Villanueva J, Herlyn M (2008) Melanoma and the tumor microenvironment. Curr Oncol Rep 10(5):439–446
Wang X, Scarfò I, Schmidts A, Toner M, Maus MV, Irimia D (2019) Dynamic profiling of antitumor activity of CAR T cells using micropatterned tumor arrays. Adv Sci 6(23):1901829
Wiggins S (2003) Introduction to applied nonlinear dynamical systems and chaos, vol 2. Springer, Berlin
Yamamoto Y, Offord CP, Kimura G, Kuribayashi S, Takeda H, Tsuchiya S, Shimojo H, Kanno H, Bozic I, Nowak MA et al (2016) Tumour and immune cell dynamics explain the PSA bounce after prostate cancer brachytherapy. Br J Cancer 115(2):195–202
Yang ZZ, Novak AJ, Ziesmer SC, Witzig TE, Ansell SM (2006) Attenuation of CD8+ T-cell function by CD4+ CD25+ regulatory T cells in B-cell non-Hodgkin's lymphoma. Cancer Res 66(20):10145–10152
Zhang G, Wang L, Cui H, Wang X, Zhang G, Ma J, Han H, He W, Wang W, Zhao Y et al (2014) Anti-melanoma activity of T cells redirected with a TCR-like chimeric antigen receptor. Sci Rep 4:3571